

1 **Nasally-delivered interferon-λ protects mice against upper and lower respiratory
2 tract infection of SARS-CoV-2 variants including Omicron**

3

4 **Authors:** Zhenlu Chong¹, Courtney E. Karl^{1,2}, Peter J. Halfmann³, Yoshihiro Kawaoka^{3,4,5},
5 Emma S. Winkler^{1,6}, Jinsheng Yu⁷, and Michael S. Diamond^{1,2,6,8} ¶||

6

7 ¹Department of Medicine, Washington University School of Medicine, St. Louis, St. Louis, MO, USA

8 ²Department of Molecular Microbiology, Washington University School of Medicine, St. Louis, MO,
9 USA

10 ³Influenza Research Institute, Department of Pathobiological Sciences, School of Veterinary Medicine,
11 University of Wisconsin-Madison, Madison, WI, USA.

12 ⁴Division of Virology, Institute of Medical Science, University of Tokyo, Tokyo, Japan

13 ⁵The Research Center for Global Viral Diseases, National Center for Global Health and Medicine
14 Research Institute, Tokyo, Japan.

15 ⁶Department of Pathology and Immunology, Washington University School of Medicine, St. Louis, St.
16 Louis, MO, USA

17 ⁷Department of Genetics, Washington University School of Medicine, St. Louis, St. Louis, MO, USA

18 ⁸The Andrew M. and Jane M. Bursky Center for Human Immunology and Immunotherapy
19 Programs, Washington University School of Medicine, St. Louis, St. Louis, MO, USA

20

21

22 ¶ **Corresponding author:** Michael S. Diamond, M.D., Ph.D., mdiamond@wustl.edu

23 **Lead Contact:** Michael S. Diamond, M.D., Ph.D.

24

25

26 **SUMMARY**

27 Although vaccines and monoclonal antibody countermeasures have reduced the
28 morbidity and mortality associated with SARS-CoV-2 infection, variants with constellations
29 of mutations in the spike gene threaten their efficacy. Accordingly, antiviral interventions that
30 are resistant to further virus evolution are needed. The host-derived cytokine IFN- λ has been
31 proposed as a possible treatment based on correlative studies in human COVID-19 patients.
32 Here, we show IFN- λ protects against SARS-CoV-2 B.1.351 (Beta) and B.1.1.529 (Omicron)
33 variants in three strains of conventional and human ACE2 transgenic mice. Prophylaxis or
34 therapy with nasally-delivered IFN- λ 2 limited infection of historical or variant (B.1.351 and
35 B.1.1.529) SARS-CoV-2 strains in the upper and lower respiratory tracts without causing
36 excessive inflammation. In the lung, IFN- λ was produced preferentially in epithelial cells and
37 acted on radio-resistant cells to protect against of SARS-CoV-2 infection. Thus, inhaled
38 IFN- λ may have promise as a treatment for evolving SARS-CoV-2 variants that develop
39 resistance to antibody-based countermeasures.

40

41 **INTRODUCTION**

42 Severe acute respiratory syndrome coronavirus 2 (SARS-CoV-2) emerged in 2019 and
43 has infected more than 300 million people worldwide. The coronavirus disease 2019
44 (COVID-19) pandemic continues because of the evolution of highly transmissible variant
45 strains and a failure to vaccinate large segments of the global population. SARS-CoV-2
46 infection causes a range of influenza-like symptoms but can progress rapidly to pneumonia,
47 acute respiratory distress syndrome (ARDS), and death (Guan et al., 2020; Huang et al.,
48 2020).

49 One hallmark of COVID-19 in some individuals is a hyper-inflammatory state with
50 excessive production of proinflammatory mediators, which recruit activated immune cells
51 that ultimately impair alveolar gas-exchange and injure the lung (Mehta et al., 2020; Zhang et
52 al., 2020). Interferons (IFNs) are pro-inflammatory cytokines that are a first line of defense
53 against most virus infections. Type I (IFN- α subtypes and IFN- β) and type III IFNs (IFN- λ s)
54 are induced rapidly after detection by and activation of pathogen sensors (*e.g.*, Toll-like [TLR]
55 or RIG-I-like [RLR] receptors) and their downstream signaling pathways (Park and Iwasaki,
56 2020). Type I and III IFNs bind to distinct receptors on the cell surface to activate signal
57 transducers and activators of transcription (STATs) proteins that induce expression of
58 hundreds of antiviral IFN-stimulated genes (ISGs) (Lazear et al., 2019; Schneider et al.,
59 2014). Cell culture studies have shown that IFN pre-treatment can restrict SARS-CoV-2
60 infection in human intestinal and airway epithelia (Felgenhauer et al., 2020; Stanifer et al.,
61 2020; Vanderheiden et al., 2020). Although type I IFNs are a potential treatment strategy for
62 SARS-CoV-2 infection (Hoagland et al., 2021), the ubiquitous expression of the

63 IFNAR1/IFNAR2 receptor and strong, sustained pro-inflammatory responses can have
64 pathological consequences. In comparison, the cellular response to type III IFN- λ is thought
65 to be less inflammatory, as it functions primarily at epithelial and barrier surfaces where its
66 heterodimeric receptor (IFNLR1/IL10R β) is preferentially expressed (Andreakos and
67 Tsiodras, 2020; Broggi et al., 2020b; Galani et al., 2017).

68 The role of IFN- λ in SARS-CoV-2 infection and pathogenesis remains unclear. Although
69 patients with severe COVID-19 patients have elevated serum levels of pro-inflammatory
70 cytokines and chemokines, generally, their type I and III IFN levels are lower (Blanco-Melo
71 et al., 2020; Galani et al., 2021), which suggests possible virus-induced antagonism or
72 skewing of antiviral responses. Notwithstanding this point, in one human study, higher serum
73 IFN- λ levels were associated with less viral infection in the respiratory tract and more rapid
74 viral clearance, and a higher IFN- λ to type I IFN ratio correlated with improved outcome
75 (Galani et al., 2021). In the respiratory tract, IFN- λ expression varies with location, level of
76 viral burden, and degree of disease severity, and may have opposing roles at distinct
77 anatomical sites in COVID-19 patients (Sposito et al., 2021). Thus, while IFN- λ expression
78 appears to correlate inversely with COVID-19 severity, its mechanism(s) of protection is not
79 well understood. Although IFN- λ has been studied in animals in the context of SARS-CoV-2
80 infection (Boudewijns et al., 2020; Broggi et al., 2020a; Dinnon et al., 2020; Sohn et al.,
81 2021), and postulated to have a protective antiviral role, the responding cell types and targets
82 of action have not been identified.

83 The emergence of SARS-CoV-2 variants (Beta, B.1.351; Gamma, B.1.1.28, Delta,
84 B.1.617.2; and Omicron, B.1.1.529) with increasing antigenic divergence in the spike protein

85 has highlighted a need for broad-spectrum antiviral agents that are less sensitive to viral
86 evolution and the development of resistance. Hence, the potential benefits of host-target
87 therapies, such as IFN- λ , have been discussed (Andreakos and Tsiodras, 2020;
88 Prokunina-Olsson et al., 2020). Here, we investigated the potential efficacy of IFN- λ in the
89 context of SARS-CoV-2 infection in mice. We found that *Ifnlr1*^{-/-} (also termed IL28R α ^{-/-})
90 C57BL/6 mice infected with B.1.351 or B.1.1.529 variants sustained higher viral burdens in
91 the respiratory tract, indicating a protective role for IFN- λ against SARS-CoV-2 infection.
92 When we administered recombinant murine IFN- λ 2 by an intranasal route to K18-human
93 (h)ACE2 transgenic mice or conventional 129S2 mice, as prophylaxis or therapy, we
94 observed markedly reduced upper and lower respiratory tract infection and inflammation.
95 Administration of nasally-delivered IFN- λ 2 several days before or after infection conferred
96 protection against infection in the lungs. IFN- λ was produced principally in epithelial cells
97 and acted mainly on radio-resistant cells. Our data in mice suggest that IFN- λ has therapeutic
98 potential as a less inflammatory, broad-spectrum antiviral agent against SARS-CoV-2 and its
99 emerging variants.

100

101 **RESULTS**

102 **IFN-λ signaling contributes to the antiviral response against SARS-CoV-2.** To assess
103 the importance of IFN-λ signaling in protection against SARS-CoV-2 infection, we
104 inoculated 6-week-old wild-type (WT) and congenic *Ifnlr1*^{-/-} C57BL/6 mice with 10⁵
105 focus-forming units (FFU) of SARS-CoV-2 B.1.351 virus, which contains K417Y, E484K,
106 and N501Y substitutions in the spike receptor-binding domain (RBD) (Tegally et al., 2021).
107 Prior studies have shown that the N501Y change in spike is mouse-adapting and can enable
108 binding to mouse ACE2 and infection of several laboratory strains of mice (Chen et al.,
109 2021a; Li et al., 2021; Rathnasinghe et al., 2021; Shuai et al., 2021; Winkler et al., 2021;
110 Zhang et al., 2021a). *Ifnlr1*^{-/-} mice showed higher viral RNA levels at 7 days post infection
111 (dpi) in nasal washes and lung homogenates compared to WT mice (**Fig 1A**). Consistent with
112 these data, we detected substantially higher levels of infectious virus by plaque assay in the
113 lungs of *Ifnlr1*^{-/-} mice at 7 dpi (**Fig 1B**). Next, we investigated whether IFN-λ also had
114 protective effects against the emerging SARS-CoV-2 B.1.1.529 Omicron variant, which has
115 mutations that could enable evasion against vaccines and therapeutic antibodies (Zhang et al.,
116 2021b). We inoculated 3-month-old WT and *Ifnlr1*^{-/-} mice with 10⁵ FFU of B.1.1.529 and
117 observed that *Ifnlr1*^{-/-} mice sustained higher levels of viral RNA in nasal turbinates, nasal
118 washes, and lungs at 5 dpi (**Fig 1C**). Infectious virus titers also were higher in *Ifnlr1*^{-/-} than
119 WT mice in both nasal turbinates and lung homogenates (**Fig 1D**). Collectively, these data
120 suggest that IFN-λ signaling has an antiviral role during SARS-CoV-2 variant infection in
121 C57BL/6 mice.

122 **Exogenous IFN-λ2 limits SARS-CoV-2 virus infection and inflammation in**

123 **K18-hACE2 transgenic mice.** We next evaluated the protective activity of exogenous
124 IFN-λ2 against SARS-CoV-2 infection in mice. In a first set of experiments, we used
125 K18-hACE2 transgenic mice, which express hACE2 under regulation of the epithelial cell
126 cytokeratin-18 promoter and are highly vulnerable to SARS-CoV-2-induced pneumonia and
127 brain infection (Golden et al., 2020; Oladunni et al., 2020; Winkler et al., 2020). We first
128 administered 2 µg of commercially-available IFN-λ2 via intranasal or intraperitoneal route 16
129 h before inoculation with a historical WA1/2020 D614G SARS-CoV-2 strain. At 3 dpi, mice
130 treated with IFN-λ2 by an intranasal route had markedly lower levels of viral RNA and
131 infectious virus in the nasal turbinates, nasal washes, lungs, and brain (**Fig S1B-C**), whereas
132 animals treated by an intraperitoneal route did not show these reductions (**Fig S1A**). Based on
133 these data, we used intranasal administration of IFN-λ2 for the remainder of our studies. We
134 extended the window of prophylaxis in K18-hACE2 mice with a single intranasal dose of
135 IFN-λ2 at day -2 (D-2) or -3 (D-3) before inoculation with WA1/2020 D614G. IFN-λ2
136 treatment at D-2 resulted in lower viral RNA levels in nasal turbinates, nasal washes, and
137 lungs, but not in the brain at 3 dpi (**Fig 2A and S2A**). Infectious virus levels in the lungs of
138 IFN-λ2-treated animals were lower than in PBS-treated animals; however, there was no
139 difference in the nasal turbinates of these two groups (**Fig 2B**). D-3 treatment with IFN-λ2
140 showed reduced viral RNA and infectious virus levels in the lungs at 3 dpi but not in other
141 tissues (**Fig S1D-E**). Finally, we tested whether protection could be improved with two doses
142 of IFN-λ2 treatment, one administered before and a second given after virus inoculation.
143 K18-hACE2 mice were treated with 2 µg of IFN-λ2 via intranasal route at 16 h before and 8
144 h after intranasal inoculation with 10^3 FFU of WA1/2020 D614G. Notably, IFN-λ2 treatment

145 prevented weight loss (**Fig S1H**) and showed reduced levels of viral RNA and infectious
146 virus at 7 dpi in the nasal turbinates, nasal washes, lungs and brain compared to PBS-treated
147 mice (**Fig S1I-J**).

148 We next explored the therapeutic efficacy of IFN-λ2. K18-hACE2 mice were
149 administered a single 2 µg dose of IFN-λ2 via nasal route at 8 h after infection, and animals
150 were sacrificed at 3 dpi. IFN-λ2 treated mice showed reduced viral RNA levels in the nasal
151 turbinates, lungs, and brain (**Fig S1F**), and infectious virus titers in the nasal turbinates and
152 lungs (**Fig S1G**). However, therapeutic administration of IFN-λ2 did not reduce viral burden
153 in nasal washes compared to PBS-treated animals (**Fig S1F**). We also administered IFN-λ2 as
154 a two-dose therapy at 1 (D+1) and 2 (D+2) dpi, which resulted in lower viral RNA loads in
155 nasal turbinates and lungs, but not in nasal washes or the brain (**Fig 2C and S2B**). Infectious
156 virus levels also were lower in the lungs with this IFN-λ2 treatment scheme (**Fig 2D**).

157 Some COVID-19 patients develop hyper-inflammatory immune responses, which may
158 contribute to respiratory failure (Andreakos and Tsiodras, 2020; Galani et al., 2021). Given
159 that IFN-λ2 treatment reduced viral levels in the lung, we hypothesized that it also might
160 mitigate immune responses and lung disease. Lung tissues were collected from IFN-λ2 or
161 PBS-treated mice at 7 dpi and sectioned for histological analysis; this time point was selected
162 since lung pathology in K18-hACE2 mice is greater at 7 than 3 dpi. Lungs from PBS-treated,
163 SARS-CoV-2-infected K18-hACE2 mice showed diffusely infiltrating immune cells with
164 alveolar space consolidation consistent with pneumonia, whereas this was observed to a
165 substantially lesser degree in IFN-λ2-treated animals (**Fig 2E**). Measurement of cytokine and
166 chemokines in lung homogenates at 3 dpi showed decreased levels of G-CSF, IL-1β, IL-6,

167 CXCL10, CCL2, and TNF- α in IFN- λ 2-treated K18-hACE2 mice (**Fig 2F and S3**). These
168 results suggest that treatment with IFN- λ 2 can protect mice against SARS-CoV-2 by
169 inhibiting lung infection and inflammation.

170 We evaluated whether exogenous IFN- λ 2 treatment could also protect K18-hACE2 mice
171 from the B.1.1.529 Omicron variant. First, we administered mice a single 2 μ g dose of
172 IFN- λ 2 at D-1. IFN- λ 2 treated mice had lower levels of B.1.1.529 viral RNA in nasal
173 turbinates, nasal washes and lungs (**Fig 2G**) as well as infectious virus in lungs than
174 PBS-treated animals (**Fig 2H**). Our two-dose therapeutic regimen at D+1 and D+2 also
175 reduced levels of B.1.1.529 viral RNA and infectious virus in the lungs, but not in the nasal
176 turbinates or washes (**Fig 2I-J**). While performing these studies, we observed an absence of
177 viral RNA in the brain of PBS-treated B.1.1.529-infected K18-hACE2 mice (**Fig S2C-D**) and
178 low levels of infection in nasal turbinates (**Fig 2H and J**), which is consistent with recent
179 studies suggesting B.1.1.529 is less pathogenic in rodents (Diamond et al., 2021).
180 Nonetheless, our experiments demonstrate that exogenous IFN- λ 2 protects against B.1.1.529
181 infection in K18-hACE2 mice.

182 **Exogenous IFN- λ 2 limits SARS-CoV-2 infection and inflammation in 129S2 mice.**
183 To confirm our results in another model of SARS-CoV-2 infection, we treated and challenged
184 129S2 mice, which are susceptible to SARS-CoV-2 strains (*e.g.*, B.1.351) with an N501Y
185 mouse-adapting mutation, more so than C57BL/6 mice (Chen et al., 2021a; Li et al., 2021;
186 Rathnasinghe et al., 2021; Shuai et al., 2021; Zhang et al., 2021a). Nasal administration of
187 IFN- λ 2 at D-1 protected B.1.351-infected mice from weight loss (**Fig 3A**) and reduced viral
188 burden in nasal turbinates, nasal washes, lungs, and brain (**Fig 3B-C and S2E**). When we

189 extended the prophylaxis window to D-3 or D-5, IFN-λ2 still reduced infection-induced
190 weight loss (**Fig 3D and G**) and viral RNA and infectious virus levels in nasal turbinates and
191 lungs, but not in nasal washes (**Fig 3E, F, H and I**). 129S2 mice treated at D-3 but not D-5
192 with IFN-λ2 had less viral RNA in the brain than those administered PBS (**Fig S2F-G**). We
193 next evaluated the effect of two 2-μg doses of IFN-λ2 -16 h and +8 h infection on B.1.351
194 infection. Infected 129S2 mice treated with PBS showed about 15% weight loss by 4 dpi,
195 whereas IFN-λ2 treated animals did not (**Fig 3J**). Levels of viral RNA and infectious virus
196 levels were reduced in the nasal turbinates, nasal washes, lungs, and brain of IFN-λ2-treated
197 compared to PBS-treated mice (**Fig 3K-L and S2H**).

198 Lung sections from B.1.351-infected, PBS-treated 129S2 mice at 4 dpi showed mild to
199 moderate immune cell infiltration, extravasation of erythrocytes into the alveolar space, and
200 pulmonary vascular congestion, whereas those treated with IFN-λ2 appeared more like
201 uninfected, naïve mice (**Fig 3M**). Consistent with these data, IFN-λ2 treated mice had
202 reduced levels of the pro-inflammatory cytokines and chemokines that were elevated in
203 B.1.351-infected PBS treated mice including IL-1β, IL-6, CXCL10, CCL2, CCL4, and CCL5
204 (**Fig 3N and S4**). Collectively, our data establishes a protective effect of IFN-λ2 against
205 SARS-CoV-2 infection in multiple strains of mice.

206 **IFN-λ2 transcriptional signature in the lung.** To begin to understand how IFN-λ2
207 protects against SARS-CoV-2 in the lung, we performed bulk RNA sequencing on tissues
208 obtained from naïve animals or animals treated IFN-λ2 via the intranasal route. Principal
209 component analysis showed distinct transcriptional signatures in the lungs of IFN-λ2-treated
210 mice at 1 (D+1) or 3 (D+3) day(s) after treatment compared to naïve mice. The

211 transcriptional signature in the lung at D+1 after IFN-λ2 was distinct from naïve animals,
212 whereas by D+3 the signature started to return to baseline (**Fig 4A**). We identified 1,820 and
213 1,317 differentially expressed genes (DEGs) in the D+1 and D+3 IFN-λ2-treated groups,
214 respectively, and 856 DEGs were identified between the D+1 and D+3 groups (**Fig 4B**). We
215 performed Metascape analysis to define biological pathways enriched in the IFN-λ2-treated
216 groups compared to naïve group. Among the top enriched up-regulated pathways in both the
217 D+1 and D+3 groups relative to the naïve group were extracellular matrix organization
218 signaling (e.g., *Col2a1*, *Col5a2*, *Lampb3*, and *Mmp15*), regulation of cell adhesion signaling
219 (e.g., *Vegfc*, *Jam2*, and *Cav1*), response to wounding signaling (e.g., *CD36*, *Tim1*, and
220 *Col3a1*), and negative regulation of cytokine production signaling (e.g., *Klf2*, *Arg2*, and
221 *Foxj1*) (**Fig 4C-D and S5**). Although these pathways were enriched in both groups,
222 expression of these genes in D+3 group was lower (**Fig 4C-D and S5**), suggesting the effect
223 of IFN-λ2 had begun to wane. In comparison, other transcriptional programs were uniquely
224 expressed in D+1 group including response to IFN-α signaling (e.g., *Oas1a*, *Ifit2*, and *Bsl2*)
225 and virus signaling (e.g., *Cxcl10*, *Rsad2*, *Isg15*, *Irf7*, and *Ifit1*) (**Fig 4C-D**), suggesting these
226 antiviral signals are induced quickly and decline rapidly once the stimulus is lost. Other
227 pathways transcriptionally induced by IFN-λ2 at D+1 only included T cell mediated
228 cytotoxicity signaling (e.g., *H2-q1*, *H2-q7*, *H2-k1*, and *Tap2*) and morphogenesis of a
229 branching epithelium signaling (e.g., *Wnt2*, *Foxc2*, and *Myc*) (**Fig 4C-D and S5**). Biological
230 pathways that were downregulated in D+1 and D+3 groups compared to naïve samples
231 included sodium ion transport signaling, protein citrullination signaling and potassium ion
232 transmembrane transport signaling. Some pathways that were downregulated only in the D+1

233 group included responses to xenobiotic stimulus signaling and negative regulation of lipid
234 metabolic process signaling (e.g., *Apobec1*, *Serpina12* and *Gper1*).

235 We validated our bulk RNA sequencing data by qRT-PCR by measuring expression of
236 several ISGs including *Ifit1*, *Isg15*, and *Rsad2* that can respond to IFN-λ signaling (Jilg et al.,
237 2014; Lazear et al., 2019; Shindo et al., 2013). Notably, these ISGs expression levels were
238 upregulated at D+1 and diminished at D+3 (**Fig 4E**). We did not observe changes in mRNA
239 expression of *Ace2*, which can be modulated by type I IFN (Ziegler et al., 2020), or *Tmprss2*
240 (**Fig 4E**), two key genes involved in SARS-CoV-2 attachment and entry, suggesting they do
241 not respond to IFN-λ signals in mice. Collectively, our data demonstrate that the
242 transcriptional program induced by IFN-λ2 is characterized by a short burst of expression of
243 antiviral, cell-to-cell communication, and wound healing gene programs. However, we did
244 not observe higher levels of NF-κB genes (e.g., *Il6*, *Il1β* and *Tnfα*), which can be strongly
245 induced by type I IFN (Galani et al., 2017), indicating IFN-λ selectively induces antiviral but
246 not highly pro-inflammatory genes.

247 **IFN-λ is preferentially produced by epithelial cells during SARS-CoV-2 infection.**

248 We investigated which cell type(s) in the lung produce IFN-λ after SARS-CoV-2 infection *in*
249 *vivo*. *Ifnl2* and *Ifnl3* mRNA expression levels was upregulated at 2 dpi after WT C57BL/6
250 mice were inoculated with 10⁶ FFU of B.1.351 (**Fig 5A**). To identify the cell types expressing
251 IFN-λ mRNA, at 2 dpi we sorted under BSL3 conditions lung epithelial cells (ECs) and
252 different immune cells populations (alveolar macrophages (AM), monocytes (Mo),
253 neutrophils (Nφ), B cells (B), T cells (T), and dendritic cells (DC)) and then performed
254 qRT-PCR for the two IFN-λ transcripts in mice (**Fig 5B and S6**). CD45⁻CD326⁺ lung ECs

255 had the highest levels of *Ifnl2* and *Ifnl3* mRNA expression with CD45⁺CD11c⁺ Siglec
256 FMHCII⁺ DCs showing the next highest expression; the other cell types analyzed had limited
257 mRNA expression of *Ifnl2* and *Ifnl3* (Fig 5C). As expected, based on the literature (Galani et
258 al., 2017; Lazear et al., 2019), the *Ifnlrl1* receptor was expressed mainly on CD45⁻CD326⁺
259 ECs and CD45⁺CD11b⁺Ly6G⁺ N ϕ (Fig 5C). To corroborate these results, we utilized
260 *Ifnl2-Egfp* reporter mice (Galani et al., 2017) to evaluate IFN- λ expression. EGFP was greatly
261 induced at 2 dpi and localized mostly to CD326⁺ ECs lining the bronchial walls; however, we
262 did not observe substantial EGFP signal in the lung parenchyma (Fig 5D). We also
263 investigated the tropism of SARS-CoV-2 B.1.351 after infection in the lung.
264 Immunofluorescence microscopy for SARS-CoV-2 nucleocapsid showed that virus localized
265 to airway tract epithelium and co-localized with CD326⁺ ECs (Fig 5E). This pattern suggests
266 that ECs are the dominant cell type targeted for infection by SARS-CoV-2 and major source
267 of IFN- λ production in the lower respiratory tract

268 We next evaluated which pathogen recognition receptor signaling pathways induced
269 IFN- λ expression. Since IFNs can be activated through TLRs, RLRs, or cGAS-STING
270 pathways after viral infections (Park and Iwasaki, 2020), we repeated B.1.351 infection
271 experiments in *Mavs*^{-/-}, *cGas*^{-/-} and *Myd88*^{-/-} C57BL/6 mice. At 2 dpi, levels of *Ifnl2* and *Ifnl3*
272 mRNA in the lung were remarkably decreased in both *Mavs*^{-/-} and *Myd88*^{-/-} mice, but not in
273 *cGas*^{-/-} mice compared to WT mice (Fig 5F). Viral RNA levels were relatively equivalent
274 among different mouse genotypes at this early time point (Fig 5E), suggesting the differences
275 in IFN- λ expression levels were not skewed by effects on viral burden, and that the antiviral
276 effect conferred by IFN- λ in the lung requires several days to manifest. Overall, our data

277 suggest that in the lungs of mice after SARS-CoV-2 infection, IFN- λ is produced principally
278 by epithelial cells though both MAVS and MyD88-dependent signaling pathways.

279 **IFN- λ signaling in radio-resistant cells controls SARS-CoV-2 infection in the lung.**

280 As our RT-PCR data demonstrated, in the lung, IFN- λ receptors (IFNLR1/IL10R β) are
281 expressed in epithelial cells and some immune cells including neutrophils (Broggi et al., 2017;
282 Lazear et al., 2019). To determine which cell type contributed to the protective effect
283 mediated by IFN- λ against SARS-CoV-2 *in vivo*, we first depleted circulating neutrophils
284 with anti-Ly6G [1A8 mAb] in the context of IFN- λ 2 treatment (**Fig S7A**). Depletion of
285 neutrophils had no impact on the reduction in weight loss or viral burden conferred by
286 IFN- λ 2 (**Fig 6A-C**). We next generated reciprocal sets of chimeric animals in which the
287 radio-resistant compartment or radio-sensitive hematopoietic cells lacked that capacity for
288 IFN- λ signaling using donor WT or *Inflrl1*^{-/-} bone marrow and sublethally irradiated WT or
289 *Inflrl1*^{-/-} recipient mice (**Fig 6D and S7B**). Animals lacking IFN- λ signaling in the
290 radio-resistant compartment sustained similar levels of infection in the nasal washes as fully
291 *Ifnlrl1*^{-/-} mice, whereas animals lacking IFN- λ signaling in hematopoietic cells had similar
292 levels of viral RNA as mice with intact IFN- λ signaling in all cells (**Fig 6E**). In the lungs, the
293 similar trends were observed with higher levels of viral RNA in animals lacking *Ifnlrl1* in the
294 radio-resistant cell compartment (**Fig 6E**). In the nasal turbinates, the data was more nuanced,
295 where both radio-resistant and radio-sensitive *Ifnlrl1* signaling cell populations appear to
296 contribute to IFN- λ -dependent control of SARS-CoV-2 infection (**Fig 6E**). Overall, our data
297 suggest IFN- λ signaling protects mice against SARS-CoV-2 infection and depends
298 dominantly on signaling in radio-resistant cells in the lung.

299

300 **DISCUSSION**

301 In humans and other animals, SARS-CoV-2 targets the respiratory tract, which can result
302 in the development of pneumonia, ARDS, and death (Guan et al., 2020; Huang et al., 2020).
303 While existing neutralizing antibodies and vaccines against SARS-CoV-2 have conferred
304 protection for many individuals, their efficacy is jeopardized by emerging variants that have
305 increasing numbers of amino acid substitutions in the spike protein (Baum et al., 2020; Chen
306 et al., 2021b; Hoffmann et al., 2021; Liu et al., 2021). Thus, therapeutic approaches are
307 needed that can overcome viral resistance. IFN- λ induces hundreds of ISGs and has
308 protective functions against many different virus infections, at least in cell culture and animal
309 models (Lazear et al., 2019; Park and Iwasaki, 2020). Also, IFN- λ preferentially functions at
310 mucosal sites including the respiratory tract because of the selected cellular expression of
311 IFNLR1, a subunit of its receptor (Broggi et al., 2020b; Lazear et al., 2019). While type I IFN
312 is also antiviral and has greater potency, treatment is often associated with collateral systemic
313 effects and inflammation. For these reasons, we investigated the potential of IFN- λ in
314 preventing and treating SARS-CoV-2 infection. Our data in mice show that IFN- λ can protect
315 against infection by two variants (B.1.351 and B.1.1.529) and diminish inflammatory
316 responses in the lung. In the context of SARS-CoV-2 infection, IFN- λ in the lung was
317 produced primarily by ECs and acted on radio-resistant cells to confer protection.

318 Host-derived innate immune responses have the potential to limit the impact of viral
319 evolution since multiple genes and pathways contribute to inhibitory responses. Nonetheless,
320 virus-mediated attenuation of innate immune antiviral response occurs and is linked to
321 SARS-CoV-2 disease severity (Blanco-Melo et al., 2020; Galani et al., 2021; Sposito et al.,

322 2021). Indeed, serum IFN- λ levels are low in patients with severe COVID-19, yet those with
323 higher levels have better outcomes (Blanco-Melo et al., 2020; Galani et al., 2021). Related to
324 this, high levels of IFN- λ in the upper respiratory tract were associated with higher viral
325 burden but less disease severity, whereas patients with severe COVID-19 had elevated IFN- λ
326 levels in the lower respiratory tract (Sposito et al., 2021). In mice, we detected IFN- λ gene
327 expression in the lung within days of SARS-CoV-2 infection, and *Ifnlr1*^{-/-} mice lacking
328 IFN- λ signaling sustained higher viral burden in the upper and lower respiratory tract,
329 suggesting IFN- λ can protect against SARS-CoV-2 infection *in vivo*.

330 Because of the potential of IFN- λ as a broadly-acting therapy, we evaluated its antiviral
331 activity *in vivo*. Notably, equivalent doses of IFN- λ 2 delivered by a nasal but not systemic
332 route could limit SARS-CoV-2 infection. The basis for this disparity remains uncertain,
333 although higher doses given by a peripheral route might have protective effects, as was seen
334 by others after subcutaneous administration of pegylated forms of IFN- λ (Dinnon et al.,
335 2020). Post-exposure therapy with IFN- λ 2 also conferred protection in the lung in mice, but
336 the antiviral effects in other tissues were diminished, suggesting that once infection is
337 established in the upper airway, and viral evasion mechanisms are induced, IFN- λ 2 therapy
338 may have less benefit. By testing several key variants (B.1.351 and B.1.1.1529), we
339 established that IFN- λ 2 could protect broadly against antigenically-distinct SARS-CoV-2
340 isolates, and thus may be less susceptible to immune escape than monoclonal or
341 serum-derived antibodies (Baum et al., 2020; Chen et al., 2021a; Hoffmann et al., 2021; Liu
342 et al., 2021).

343 Even a single dose of IFN- λ at D-5 conferred mice protection, demonstrating a persistent

344 antiviral effect. The basis for this durable inhibitory effect remains uncertain especially in
345 light of our transcriptional profiling data in the lung, which showed a rapid induction and
346 then dampening of gene induction. Although further studies are warranted to define the basis
347 of the durable inhibitory effect, we speculate that the half-life of certain inhibitory ISG
348 products may be longer, transcriptional activation downstream of IFN- λ signaling may have
349 distinct kinetics in the upper airway, or immune cells may become ‘trained’ (Netea et al.,
350 2020) by IFN- λ to respond more quickly. We used soluble IFN- λ in our administration
351 scheme. It remains possible that the window of prevention and clinical utility could be
352 extended further by administration of longer-acting (e.g., pegylated) forms of IFN- λ .

353 Type I IFNs have been used to treat several viral diseases including chronic hepatitis C
354 virus (HCV) and human papillomavirus (HPV) (Lazear et al., 2019). Although type I IFNs
355 have garnered interest as a treatment strategy in COVID-19 (Palermo et al., 2021; Park and
356 Iwasaki, 2020; Schreiber, 2020), their ability to exacerbate inflammation has tempered
357 enthusiasm. One group tried to overcome this limitation by administering type I IFN by an
358 intranasal route; in hamsters, they showed that nasally-delivered type I IFN could reduce viral
359 burden, prevent virus transmission, and lower inflammation *in vivo* (Hoagland et al., 2021).
360 In our mouse models, administration of IFN- λ protected mice from infection, weight loss,
361 lung inflammation, and lung disease, suggesting that the less pro-inflammatory nature of
362 IFN- λ (Lazear et al., 2019) may have advantages as a therapeutic strategy. Our RNA
363 sequencing data also showed IFN- λ treatment induced a tissue repair transcriptional signature
364 in the lung, which contrasts with some studies showing that persistent type I or type III IFN
365 signaling can disrupt lung epithelial barriers and prevent tissue repair (Broggi et al., 2020a;

366 Major et al., 2020). Nonetheless, administration of IFN- λ later in the course of SARS-CoV-2
367 infection, when most of the disease is caused by the host response and not by viral replication,
368 could be detrimental and warrants further study.

369 By leveraging flow cytometry, qRT-PCR, and *Ifnl2-gfp* reporter mice, we found that
370 IFN- λ was produced mainly from lung ECs after SARS-CoV-2 infection. This observation
371 agrees with experiments by others after influenza A virus infection (Galani et al., 2017). We
372 also showed IFN- λ acted primarily on radio-resistant cells in the lung to confer protection
373 against SARS-CoV-2 infection, which is consistent with a recent finding (Broggi et al.,
374 2020a). While others have suggested that IFN- λ signaling in neutrophils is required for
375 optimal antifungal or antiviral defenses or limiting tissue damage (Broggi et al., 2017;
376 Espinosa et al., 2017; Galani et al., 2017), our neutrophil depletion studies showed no effect
377 on IFN- λ -mediated protection against SARS-CoV-2 infection or weight loss in mice. The
378 basis for the difference is uncertain but could be due to the disparate models of pathogen
379 infection or inflammation.

380 Although our experiments establish a role for IFN- λ in protecting against infection by
381 SARS-CoV-2 strains including B.1.1.529, we acknowledge several limitations to our study:
382 (a) We used female mice in our IFN- λ treatment models, so studies in male animals are
383 needed to exclude sex-based differences in therapeutic effects. Notwithstanding this, another
384 group recently showed protective effects of IFN- λ against SARS-CoV-2-induced death in
385 male K18-hACE2 mice (Sohn et al., 2021); (b) The relationship between induction of IFN- λ
386 responses in mice and COVID-19 patients is unclear, especially given that many patients with
387 severe disease have blunted IFN responses. While some of the diminished type I IFN

388 response may be due to autoantibodies (Bastard et al., 2020; van der Wijst et al., 2021), the
389 presence of such inhibitors against IFN- λ has not been described; (c) Although our neutrophil
390 deletion and bone marrow chimera studies suggest that radio-resistant cells respond to IFN- λ
391 to confer a protective antiviral effect, the precise cell type was not defined. Future studies
392 with *Ifnlrl*^{fl/fl} conditional knockout mice are required to fully answer this question; and (d)
393 Our studies are restricted to mice. IFN- λ treatment experiments in other animals (e.g.,
394 hamsters, ferrets, or nonhuman primates) and ultimately humans are needed for corroboration
395 and determination of clinical utility.

396 In summary, we present evidence that nasal administration of IFN- λ confers pre- and
397 post-exposure protection against infection by several SARS-CoV-2 strains including key
398 variants of concern without causing extensive inflammation. In the lung, IFN- λ is induced in
399 a MAVS and MyD88-dependent manner primarily in ECs that are likely infected, and acts
400 upon radio-resistant cells to control infection. Additional treatment studies are warranted to
401 evaluate further the potential of IFN- λ as a broadly-acting antiviral agent against
402 SARS-CoV-2 and its emerging variants.

403

404 **Acknowledgements.** This study was supported by grants and contracts from NIH: R01
405 AI157155, U01 AI151810, and 75N93019C00051 [all to M.S.D.], 75N93021C00014 [to Y.K.],
406 F30 AI152327 [to E.S.W.], and T32GM139774-01 [to C.E.K.].

407 **Author Contributions.** Z.C. and C.E.K. performed the infection experiments in mice.
408 Z.C. and E.S.W. titrated virus in tissues. Z.C. analyzed inflammation and pathology. J.Y.
409 analyzed the RNAseq data. P.J.H. and Y.K. isolated and propagated the B.1.1.529 isolate.
410 M.S.D. obtained funding and supervised research. Z.C. and M.S.D. wrote the initial draft,
411 with all other authors providing editorial comments.

412 **Declaration of Interests.** M.S.D. is a consultant for Inbios, Vir Biotechnology, Senda
413 Biosciences, and Carnival Corporation, and on the Scientific Advisory Boards of Moderna and
414 Immunome. The Diamond laboratory has received unrelated funding support in sponsored
415 research agreements from Moderna, Vir Biotechnology, and Emergent BioSolutions. Y.K. has
416 received unrelated funding support from Daiichi Sankyo Pharmaceutical, Toyama Chemical,
417 Tauns Laboratories, Inc., Shionogi & Co. LTD, Otsuka Pharmaceutical, KM Biologics,
418 Kyoritsu Seiyaku, Shinya Corporatoin, and Fuji Rebio.

419

420 **FIGURE LEGENDS**

421 **Figure 1. Increased susceptibility of *IfnlrI*^{-/-} mice to SARS-CoV-2 infection. (A-B)**

422 Six-week-old male and female C57BL/6 WT and *IfnlrI*^{-/-} mice were inoculated with 10⁵ FFU
423 of B.1.351. **(A)** Viral RNA levels were measured from tissues at 7 dpi by qRT-PCR. **(B)**
424 Infectious virus was measured from tissues by plaque assay at 7 dpi (n = 9-11 per group, 2
425 experiments). **(C-D)** Three-month-old female and male C57BL/6 WT and *IfnlrI*^{-/-} mice were
426 inoculated with 10⁵ FFU of B.1.1.529. **(C)** Viral RNA levels were measured at 5 dpi by
427 qRT-PCR. Note, an earlier time point of analysis was used because B.1.1.529 is less
428 pathogenic in mice. **(D)** Infectious virus was measured by plaque assay at 5 dpi (n = 8-11 per
429 group, 2 experiments). Bars indicate median values. Data were analyzed by Mann-Whitney
430 test (*P < 0.05, **P < 0.01, ***P < 0.001, and ****P < 0.0001).

431 **Figure 2. Nasally-delivered IFN-λ2 treatment protects K18-hACE2 mice against**

432 **SARS-CoV-2 infection.** Eight-week-old female K18-hACE2 mice were inoculated by
433 intranasal route with 10³ FFU of WA1/2020 D614G. At D-2 **(A-B)** or D+1 and D+2 **(C-D)**,
434 mice were given a single 2 µg dose of murine IFN-λ2 or PBS by the intranasal route. **(A and**
435 **C)** Viral RNA levels were measured at 3 dpi. **(B and D)** Infectious virus was measured at 3
436 dpi **(A-B: n = 9 per group, 2 experiments; C-D: n = 8 per group, 2 experiments).** **(E)**
437 Hematoxylin and eosin staining of lung sections from animals treated with 2 µg doses of
438 murine IFN-λ2 or PBS by intranasal route at -16 h and +8 h relative to inoculation with
439 WA1/2020 D614G and harvested at 7 dpi. Low (top, scale bars, 500 µm) and high (bottom,
440 scale bars, 100 µm) power images are shown. Representative images from n = 5 per group. **(F)**
441 Eight-week-old female K18-hACE2 mice were treated with 2 µg of murine IFN-λ2 or PBS at

442 -16 h and challenged with 10^3 FFU of WA1/2020 D614G. Heat-maps of cytokine levels in
443 lung homogenates at 3 dpi. Fold-change was calculated relative to mock-infected mice, and
444 log₂ values are plotted (2 experiments, n = 7 per group except naïve, n = 4). (G-J)
445 Five-month-old female K18-hACE2 mice were inoculated with 10^3 FFU of B.1.1529. At D-1
446 (G-H) or D+1 and D+2 (I-J), mice were given 2 µg of murine IFN-λ2 or PBS by the
447 intranasal route. Viral RNA (G and I) and infectious (H and J) virus levels were measured at
448 3 dpi (G-H: n = 7-8 per group, 2 experiments; I-J: n = 6-7 per group, 2 experiments). Bars
449 (A-D and G-J) indicate median values. Data were analyzed by Mann-Whitney tests (A-D and
450 G-J) (*P < 0.05, **P < 0.01, ***P < 0.001, and ****P < 0.0001).

451 **Figure 3. IFN-λ2 treatment protects 129S2 mice against SARS-CoV-2 infection. (A-I)**
452 Six-week-old female 129S2 mice were inoculated by intranasal route with 10^5 FFU of
453 B.1.351. At D-1 (A-C), D-3 (D-F) or D-5 (G-I), mice were given a single 2 µg dose of
454 murine IFN-λ2 or PBS by intranasal route. (A, D, G) Weight change. (B, E, H) Viral RNA
455 levels at 4 dpi. (C, F, I) Infectious virus levels at 4 dpi (A-C: n = 7 per group, 2 experiments;
456 D-F: n = 6-8 per group, 2 experiments; G-I: n = 6-8 per group, 2 experiments). (J-L)
457 Six-week-old female 129S2 mice were inoculated by intranasal route with 10^5 FFU of
458 B.1.351. At -16 h and +8 h, mice were administered 2 µg of murine IFN-λ2 or PBS by
459 intranasal route. (J) Weight change. (K) Viral RNA levels at 4 dpi. (L) Infectious virus levels
460 at 4 dpi in (n = 8 per group, 2 experiments). (M) Hematoxylin and eosin staining of lung
461 sections at 4 dpi from animals treated in (J-L). Low (top, scale bars, 500 µm) and high
462 (bottom, scale bars, 100 µm) power images are shown (representative of n = 5 per group). (N)
463 Heat-maps of cytokine levels in lung homogenates at 4 dpi from animals treated in (J-L).

464 Fold-change was calculated compared to mock infected mice, and \log_2 values were plotted (n
465 = 8 per group except naïve n = 4, 2 experiments). Bars (**B-C**, **E-F**, **H-I** and **K-L**) indicate
466 median values. Data were analyzed by Mann-Whitney tests (**B-C**, **E-F**, **H-I** and **K-L**) or *t*
467 tests of the area under the curve (**A**, **D**, **G and J**) (* $P < 0.05$, ** $P < 0.01$, *** $P < 0.001$, and
468 **** $P < 0.0001$).

469 **Figure 4. Transcriptional signatures in the lungs of mice treated with murine**
470 **IFN-λ2. (A-D)** RNA sequencing of lung homogenates of naive female K18-hACE2 mice
471 (control) or mice treated with 2 μ g of murine IFN-λ2 by intranasal route for 1 (Day+1) or 3
472 (Day+3) days. **(A)** Three-dimensional map from principal component analysis. Each group is
473 represented by an ellipse and the color-matched solid circle, which is the centroid of each
474 group. The size of the ellipse is the centroid with one standard deviation. The dashed red lines
475 with numbers indicate the spatial distance between centroids of the 3 groups, which is
476 calculated by using the three-dimensional coordinates for the centroids. **(B)** Venn diagrams of
477 overlapping genes identified in differential expression analysis when comparing with control,
478 D+1, and D+3 groups. Numbers in the parenthesis under each comparison indicate
479 differentially expressed genes (fold-change ≥ 2 at $P < 0.05$) followed by the proportion that
480 are up- or downregulated. **(C)** The significantly enriched biological processes defined by a
481 Metascape pathway analysis tool comparing control, D+1, and D+3 groups; upregulated
482 genes (brown) or downregulated (blue) in the IFN-λ2 treated group (D+1 or D+3) compared
483 to the control group or in the D+1 group compared to the D+3 group. **(D)** Heatmaps of
484 selected biological processes enriched in the D+1 group or the D+3 group versus the control
485 group (n = 4 per group). **(E)** mRNA levels of indicated target genes were measured from the

486 lung homogenates of naive female K18-hACE2 mice or mice treated with 2 μ g of murine
487 IFN- λ 2 by intranasal route for D+1 or D+3 days (n = 8-10 per group, 2 experiments). Data in
488 (E) were analyzed by one-way ANOVA with Dunnett's post-test (* P < 0.05, ** P < 0.01, and
489 *** P < 0.001).

490 **Figure 5. IFN- λ expression *in vivo*.** (A) Six-week-old male and female C57BL/6 mice
491 were inoculated with 10^6 FFU of B.1.351. *Ifnl2* and *Ifnl3* mRNA levels from lungs were
492 measured at indicated days post infection by qRT-PCR (n = 4-9 per group, 2 experiments).
493 (B-C) Six-week-old male and female C57BL/6 mice were inoculated with 10^6 FFU of
494 B.1.351. (B) Scheme depicting cell populations isolated from lungs of B.1.351-infected mice.
495 (C) *Ifnl2*, *Ifnl3* and *Ifnlr1* mRNA expression levels from (B) were measured by qRT-PCR at 2
496 dpi (n = 4 per group, each dot represents 4 mice pooled together, 2 experiments). (D-E)
497 Six-week-old C57BL/6 or *Ifnl2-Egfp* reporter mice were inoculated with 10^6 FFU of
498 SARS-CoV-2 B.1.351. (D) Localization of EGFP and epithelial cells (ECs, CD326) in the
499 lungs of *Ifnl2-Egfp* reporter mice at 2 dpi. Frozen sections stained for GFP (green), CD326
500 (magenta), and Hoechst (blue) are shown. Scale bar: 50 μ m. (E) Localization of
501 SARS-CoV-2 positive and ECs in the lung of mice at 2 dpi. Frozen sections stained for
502 SARS-CoV-2 nucleocapsid protein (NP) (green), CD326 (magenta), and Hoechst (blue) are
503 shown. Scale bars in (D-E): 50 μ m. (F-G) Six-week-old male and female WT, *Mavs*^{-/-}, *cGas*^{-/-},
504 or *Myd88*^{-/-} C57BL/6 mice were inoculated with 10^6 FFU of B.1.351. Viral RNA levels (F) or
505 *Ifnl2* and *Ifnl3* mRNA expression levels (G) from lungs were measured at 2 dpi by qRT-PCR
506 (n = 6-10, 2 experiments). Bars in (F) indicate median values. Data in (F-G) were analyzed
507 by one-way ANOVA with Dunnett's post-test (*** P < 0.001 and **** P < 0.0001).

508 **Figure 6. IFN-λ signaling in radio-resistant cells protects against SARS-CoV-2**

509 **infection. (A-C)** Six-week-old female 129S2 mice received anti-Ly6G [1A8] or isotype
510 control antibodies by intraperitoneal injection at D-1, D+1 and D+3 relative to B.1.351
511 infection (10^5 FFU). Mice also were treated with 2 µg of murine IFN-λ2 or PBS at -16 h and
512 +8 h by the intranasal route. **(A)** Weight change. **(B)** Viral RNA levels at 4 dpi. **(C)** Infectious
513 virus levels at 4 dpi (n = 8 per group, 2 experiments). **(D)** Experimental scheme for
514 generating of WT and *Ifnlr1*^{-/-} bone marrow chimeric mice. Ten weeks after irradiation, mice
515 were inoculated by the intranasal route with 10^5 FFU of B.1.351. **(E)** Viral RNA levels at 7
516 dpi (n = 13-15 per group, 3 experiments). Bars indicate median values. Data were analyzed
517 by one-way ANOVA with Dunnett's post-test of the area under the curve **(A)** and
518 Kruskal-Wallis test with Dunnett's post-test **(B-C and E)** (*P < 0.05, **P < 0.01, ***P <
519 0.001, and ****P < 0.0001).

520

521 **SUPPLEMENTAL FIGURE LEGENDS**

522 **Figure S1. SARS-CoV-2 viral burden in infected K18-hACE2 mice, Related to**

523 **Figure 2. (A)** Eight-week-old female K18-hACE2 mice were inoculated by intranasal route

524 with 10^3 FFU of WA1/2020 D614G. At -16 h before virus inoculation, mice were given 2 μ g

525 of murine IFN- λ 2 or PBS by intraperitoneal injection. Viral RNA levels at 3 dpi (n = 6-7 per

526 group, 2 experiments). **(B-G)** Eight-week-old female K18-hACE2 mice were inoculated by

527 intranasal route with 10^3 FFU of WA1/2020 D614G. At -16 h (**B-C**), D-3 (**D-E**) or +8 h (**F-G**),

528 mice were given 2 μ g of murine IFN- λ 2 or PBS by intranasal route. Viral RNA (**B, D, and F**)

529 and infectious virus (**C, E, and G**) levels at 3 dpi (**B-C**: n = 7 per group, 2 experiments; **D-E**:

530 n = 8-9 per group, 2 experiments; **F-G**: n = 6-7 per group, 2 experiments). **(H-J)**

531 Eight-week-old female K18-hACE2 mice were treated with 2 μ g doses of murine IFN- λ 2 or

532 PBS by intranasal route at -16 h and +8 h relative to inoculation with 10^3 FFU of WA1/2020

533 D614G and harvested at 7 dpi. **(H)** Weight change was monitored daily for 7 days. **(I)** Viral

534 RNA levels at 7 dpi. **(J)** Infectious virus levels at 7 dpi (**H-J**: n = 9-10 per group, 2

535 experiments). Bars (**A-G and I-J**) indicate median values. Data were analyzed by

536 Mann-Whitney test (**A-G and I-J**) or t tests of the area under the curve (**H**) (* $P < 0.05$, ** $P <$

537 0.01, *** $P < 0.001$, and **** $P < 0.0001$).

538 **Figure S2. SARS-CoV-2 viral burden in the brains of K18-hACE2 and 129S2 mice,**

539 **Related to Figures 2 and 3. (A-D)** Eight-week-old (**A-B**) or five-month-old (**C-D**) female

540 K18-hACE2 mice were inoculated by intranasal route with 10^3 FFU of WA1/2020 D614G

541 (**A-B**) or B.1.1529 (**C-D**). At D-2 (**A**), D+1 and D+2 (**B and D**) or D-1 (**C**), mice were

542 administered 2 μ g of murine IFN- λ 2 or PBS by intranasal route. Viral RNA levels from brain

543 at 3 dpi (**A**: n = 9 per group, 2 experiments; **B**: n = 8 per group, 2 experiments; **C**: n = 7-8 per
544 group, 2 experiments; **D**: n = 6-7 per group, 2 experiments). (**E-H**) Six-week-old female
545 129S2 mice were inoculated by intranasal route with 10^5 FFU of B.1.351. At D-1 (**E**), D-3 (**F**),
546 D-5 (**G**) or -16 h and +8 h (**H**), mice were administered 2 μ g of murine IFN- λ 2 or PBS by
547 intranasal route. Viral RNA levels from brain at 4 dpi (**E**: n = 7 per group, 2 experiments; **F**: n
548 = 6-8 per group, 2 experiments; **G**: n = 6-8 per group, 2 experiments; **H**: n = 8 per group, 2
549 experiments). Bars indicate median values. Data were analyzed by Mann-Whitney test (**P <
550 0.01 and ***P < 0.001).

551 **Figure S3. Cytokine responses following IFN- λ treatment and SARS-CoV-2**
552 **infection, Related to Figure 2.** Eight-week-old female K18-hACE2 mice treated with 2 μ g
553 of murine IFN- λ 2 or PBS at -16 h by the intranasal route were challenged with 10^3 FFU of
554 WA1/2020 D614G. Cytokine levels in lung homogenates at 3 dpi (2 experiments, n = 7 per
555 group except naïve n = 4). Data were analyzed by one-way ANOVA with Tukey's multiple
556 comparison test (*P < 0.05, **P < 0.01, ***P < 0.001, and ****P < 0.0001).

557 **Figure S4. Cytokine induction following IFN- λ treatment and SARS-CoV-2**
558 **infection, Related to Figure 3.** Six-week-old female 129S2 mice treated with two doses of 2
559 μ g of murine IFN- λ 2 or PBS at -16 h and +8 h by the intranasal route were challenged with
560 10^5 FFU of B.1.351. Cytokine levels in lung homogenates at 4 dpi (n = 7 per group except
561 naïve n = 4, 2 experiments). Data analyzed by one-way ANOVA with Tukey's multiple
562 comparison test (*P < 0.05, **P < 0.01, ***P < 0.001 and ****P < 0.0001).

563 **Figure S5. Heatmaps of RNA-seq data, Related to Figure 4.** Heatmaps of selected
564 significantly upregulated or downregulated gene sets corresponding with IFN- λ 2 treatment

565 identified through GO analysis. Genes shown in each pathway are the union of the
566 differentially expressed genes (DEGs) enriched in D+1 group or D+3 group versus control
567 group (n = 4 per group). Columns represent sample groups and rows indicate genes.

568 **Figure S6. Flow cytometric gating strategy for lung cell populations, Related to**

569 **Figure 5. (A-D)** For lung tissues, cells were gated on single, live, CD45⁺ and CD45⁻ cells.
570 Alveolar macrophages (AM) were identified as CD45⁺ SiglecF^{hi} CD11c^{hi} cells, dendritic cells
571 (DC) were identified as CD45⁺ SiglecF⁻ CD11c⁺ MHCII⁺ cells (A). B and T cells were
572 identified as CD45⁺ CD19⁺ cells and CD45⁺ CD3⁺ cells, respectively (B). Neutrophils (N ϕ)
573 and epithelial cells (EC) were identified as CD45⁺CD11b⁺Ly6G⁺ cells and CD45⁻ CD326⁺
574 cells, respectively (C). Monocytes (Mo) were identified as CD45⁺ CD11b⁺ Ly6C^{hi} cells (D).

575 **Figure S7. Flow cytometry analysis of peripheral blood from neutrophil-depleted**
576 **or bone marrow chimeric mice, Related to Figure 6. (A)** Experimental scheme of
577 neutrophil deletion in 129S2 mice. **(B)** (*Left*) Representative flow cytometry plots of
578 peripheral blood at D+4 following intraperitoneal injection of a depleting anti-Ly6G mAb
579 (1A8) or isotype control mAb. (*Right*) Frequency of mature neutrophils
580 (CD11b⁺Ly6B⁺Ly6G⁺Ly6C^{int}) in blood are shown after antibody depletion (n = 8 per group, 2
581 experiments). **(C)** Representative flow cytometry plots of peripheral blood at 10 weeks after
582 irradiation and bone marrow cell transplantation of CD45.2 cells to CD45.1 recipient mice.
583

584 **STAR METHODS**

585 **RESOURCE AVAILABILITY**

586 **Lead contact.** Further information and requests for resources and reagents should be
587 directed to the Lead Contact, Michael S. Diamond (diamond@wusm.wustl.edu).

588 **Materials availability.** All requests for resources and reagents should be directed to the
589 Lead Contact author. This includes mice, antibodies, viruses, and proteins. All reagents will
590 be made available on request after completion of a Materials Transfer Agreement.

591 **Data and code availability.** All data supporting the findings of this study are available
592 within the paper and or upon request from the corresponding author. RNA sequencing
593 datasets are available for analysis (GEO accession number GSE193990).

594

595 **EXPERIMENTAL MODEL AND SUBJECT DETAILS**

596 **Cells and viruses.** Vero-TMPRSS2 and Vero-TMPRSS2-ACE2 cells (Chen et al., 2021b)
597 were cultured at 37°C in Dulbecco's Modified Eagle medium (DMEM) supplemented with 10%
598 fetal bovine serum (FBS), 10 mM HEPES pH 7.3, and 100 U/ml of penicillin–streptomycin.
599 The SARS-CoV-2 WA1/2020 D614G virus was produced from an infectious clone and has
600 been described previously (Chen et al., 2021b). The B.1.351 and B.1.1529 viruses were
601 isolated from infected individuals and have been described previously (Chen et al., 2021a;
602 VanBlargan et al., 2022). Infectious stocks were propagated in Vero-TMPRSS2 cells as
603 described (Case et al., 2020). All work with infectious SARS-CoV-2 was performed in
604 approved BSL3 and A-BSL3 facilities at Washington University School of Medicine using
605 appropriate positive pressure air respirators and protective equipment.

606 **Mice.** Animal studies were carried out in accordance with the recommendations in the
607 Guide for the Care and Use of Laboratory Animals of the National Institutes of Health. The
608 protocols were approved by the Institutional Animal Care and Use Committee at the
609 Washington University School of Medicine. Virus inoculations were performed under
610 anesthesia that was induced and maintained with ketamine hydrochloride and xylazine, and
611 all efforts were made to minimize animal suffering. WT C57BL/6J (#000664) mice were
612 obtained from The Jackson Laboratory or bred in a pathogen-free animal facility at
613 Washington University. *Ifnlr1*^{-/-} (Ank et al., 2008) and *Ifnl2-gfp* reporter mice (originally
614 generated by Evangelos Andreakos, and kindly provided by Megan Baldridge, Washington
615 University) were bred and housed in a pathogen-free animal facility at Washington University.
616 Heterozygous K18-hACE C57BL/6J mice (strain: 2B6.Cg-Tg(K18-ACE2)2Prlmn/J) were
617 obtained from The Jackson Laboratory. 129S2 mice were obtained from Charles River.
618 Animals were housed in groups and fed standard chow diets.

619

620 **METHOD DETAILS**

621 **Mouse infection, immune cell depletion and bone marrow chimeric mice studies.** For
622 neutrophil depletion, anti-Ly6G (BioXCell; clone 1A8) or an isotype control (BioXCell;
623 clone 2A3) was administered to mice by intraperitoneal injection at D-1 (500 µg), D+1 (200
624 µg) and D+3 (200 µg) relative to B.1.351 inoculation. For bone marrow chimeric mice,
625 six-week-old male and female WT (CD45.1) and *Ifnlr1*^{-/-} (CD45.2) recipient mice were
626 irradiated with 9 Gy (X-ray) total body irradiation (TBI). One day later, mice were injected
627 with 5×10^6 sex-matched bone marrow cells from donor WT (CD45.2) or *Ifnlr1*^{-/-} (CD45.2)

628 mice. Ten weeks later, peripheral blood cell from recipient chimeric mice were analyzed by
629 flow cytometry as described below.

630 **Plaque assay.** Vero-TMPRSS2-ACE2 cells were seeded at a density of 1.25×10^5 cells
631 per well in flat-bottom 24-well tissue culture plates. The following day, media was removed
632 and replaced with 200 μL of 10-fold serial dilutions of sample, diluted in DMEM+2% FBS.
633 One hour later, 1 mL of methylcellulose overlay was added. Plates were incubated for 72 h,
634 then fixed with 4% paraformaldehyde (final concentration) in PBS for 1 hour. Plates were
635 stained with 0.05% (w/v) crystal violet in 20% methanol and washed twice with distilled,
636 deionized water. Plaques were counted, and titers were calculated according to a previously
637 described method (Case et al., 2020).

638 **Measurement of viral RNA.** Mice were euthanized and tissues were collected. Nasal
639 washes were collected in 0.5 mL of PBS. Tissues were weighed and homogenized with
640 zirconia beads in a MagNA Lyser instrument (Roche Life Science) in 1 mL of DMEM media
641 supplemented with 2% FBS. Tissue homogenates were clarified by centrifugation at 10,000
642 rpm for 5 min and stored at -80 $^{\circ}\text{C}$. Viral RNA from homogenized tissues or nasal washes was
643 isolated using the MagMAX Viral RNA Isolation Kit (ThermoFisher) and measured by
644 TaqMan one-step quantitative reverse-transcription PCR (RT-qPCR) on an ABI 7500 Fast
645 Instrument. Copies of SARS-CoV-2 *N* gene RNA in samples were determined using a
646 previously published assay (Case et al., 2020). Briefly, a TaqMan assay was designed to
647 target a highly conserved region of the *N* gene (Forward primer:
648 ATGCTGCAATCGTGCTACAA; Reverse primer: GACTGCCGCCTCTGCTC; Probe:
649 /56-FAM/TCAAGGAAC/ZEN/AACATTGCCAA/3IABkFQ/). This region was included in

650 an RNA standard to allow for copy number determination down to 10 copies per reaction.
651 The reaction mixture contained final concentrations of primers and probe of 500 and 100 nM,
652 respectively.

653 **Cytokine and chemokine protein measurements.** Lung homogenates were incubated
654 with Triton X-100 (1% final concentration) for 1 h at room temperature to inactivate
655 SARS-CoV-2. Homogenates were analyzed for cytokines and chemokines by Eve
656 Technologies Corporation (Calgary, AB, Canada) using their Mouse Cytokine
657 Array/Chemokine Array 31-Plex (MD31) platform.

658 **Lung histology.** Animals were euthanized before harvest and fixation of tissues. Lungs
659 were inflated with 1.2 mL of 10% neutral buffered formalin using a 3-mL syringe and
660 catheter inserted into the trachea. Tissues were embedded in paraffin, and sections were
661 stained with hematoxylin and eosin. Images were captured using the Nanozoomer
662 (Hamamatsu) at the Alafi Neuroimaging Core at Washington University.

663 **Flow cytometry analysis of peripheral blood.** For analysis of immune cell depletion,
664 peripheral blood cells were collected, and erythrocytes were lysed with ACK lysis buffer
665 (GIBCO) and resuspended in RPMI supplemented with 10% FBS. Single cell suspensions
666 were preincubated with Fc Block antibody (BD PharMingen) in PBS + 2% FBS for 10 min at
667 room temperature before staining. Cells were incubated with antibodies against the following
668 markers: BV421 anti-CD45, AF700 anti-Ly6C, FITC anti-Ly6B, PE-CY7 anti-Ly6G and
669 APC anti-CD11b. All antibodies were used at a dilution of 1:200. Cells were stained for 20
670 min at 4 °C, washed with PBS, fixed with 4% PFA for 15 min, washed with PBS and
671 resuspended with FACS (PBS + 2% FBS + 2 mM EDTA) buffer.

672 **Lung digestion and cell sorting by flow cytometry.** Lungs were collected and digested
673 at 37°C with 5 mg/mL of collagenase I (Worthington) and 1 mg/mL of DNase I (Roche) for 45
674 min in HBSS buffer. Digested lung tissues were minced, passed through a 40 µm strainer, and
675 centrifuged at 500 g for 10 min. Red blood cells were lysed with ACK lysis buffer (GIBCO).
676 Dead cells were removed by Dead Cell Removal Kit (STEMCELL) according manufacturer's
677 protocol. Single cell suspensions were incubated with APC-CY7 anti-CD45, APC
678 anti-CD11b, BV421 anti-Ly6G, BV-421 anti-CD11c, PE anti-Siglec F (CD170), AF-700
679 anti-MHC II (I-A/I-E), BV421 anti-CD3, PE anti-CD19, APC anti-CD11b, PE anti-CD326
680 and PE anti-Ly6C antibodies as described above. AM (CD45⁺ SiglecF^{hi} CD11c^{hi}), DCs
681 (CD45⁺ SiglecF⁻ CD11c⁺ MHCII⁺), B cells (CD45⁺ CD19⁺), T cells (CD45⁺ CD3⁺), N ϕ
682 (CD45⁺ CD11b⁺ Ly6G⁺), ECs (CD45⁻ CD326⁺) and Mo (CD45⁺ CD11b⁺ Ly6C^{hi}) were sorted
683 by flow cytometry (Sony SH800Sorter) under BSL3 conditions. RNA was extracted with
684 RNeasy Micro Kit (QIAGEN) according to manufacturer's protocol and then *Ifnl2*, *Ifnl3*, and
685 *Ifnlr1* mRNA levels were measured by qRT-PCR as described above.

686 **Confocal microscopy.** Lung tissues were collected as described above and fixed for 7
687 days. Tissues then were washed three time with PBS and placed into 30% sucrose in PBS
688 overnight until sinking to the bottom of the tube. Tissues were placed into O.C.T. medium in
689 cryomolds on dry ice, wrapped in aluminum foil, and stored in -80C. Sections were cut and
690 embedded on superfrost glass slides. Slides were rinsed three times with PBS, blocked with 5%
691 FBS, 1% BSA and 0.3% Triton X-100 in PBS, and incubated with rat anti-CD326 (1: 500),
692 rabbit anti-nucleocapsid protein (1: 500), and chicken anti-GFP (1: 1000) primary antibodies
693 at 4°C overnight. The next day, slides were stained with goat anti-chicken (1: 500), donkey

694 anti-rabbit (1: 500) and donkey anti-rat (1: 500) secondary antibodies for 1 h at room
695 temperature and with Hoechst dye (1:10000) for 5 min. Slides were washed with PBS once,
696 mounted with AquaPoly, and stored in the dark at 4°C until imaged.

697 **RNA sequencing.** RNA from lung tissues was extracted by RNeasy PIs Mini Kit
698 (QIAGEN) according to manufacturer's protocol. cDNA libraries were constructed starting
699 with 10 ng of total RNA. cDNA was generated using the Seqplex kit (Sigma-Aldrich, St.
700 Louis, MO) with amplification of 20 cycles. Library construction was performed using 100
701 ng of cDNA undergoing end repair, A-tailing, ligation of universal TruSeq adapters, and 8
702 cycles of amplification to incorporate unique dual index sequences. Libraries were sequenced
703 on the NovaSeq 6000 (Illumina, San Diego, CA) targeting 40 million read pairs and
704 extending 150 cycles with paired end reads. RNA-seq reads were aligned to the mouse
705 Ensembl GRCh38.76 primary assembly with STAR program (version 2.5.1a) (Dobin et al.,
706 2013). Gene counts were derived from the number of uniquely aligned unambiguous reads by
707 Subread:featureCount (version 1.4.6-p5) (Liao et al., 2014). The ribosomal fraction, known
708 junction saturation, and read distribution over known gene models were quantified with
709 RSeQC (version 2.6.2) (Liao et al., 2014). All gene counts were preprocessed with the R
710 package EdgeR (Robinson et al., 2010) to adjust samples for differences in library size using
711 the trimmed mean of M values (TMM) normalization procedure. Viral and ribosomal genes
712 and genes not expressed in at least five samples (the smallest group size) at a level greater
713 than or equal to 1 count per million reads were excluded, resulting 19,280 unique genes in
714 further analysis. The R package limma (Ritchie et al., 2015) with voomWithQualityWeights
715 function (Liu et al., 2015) was utilized to calculate the weighted likelihoods for all samples,

716 based on the observed mean-variance relationship of every gene and sample. Differentially
717 expressed genes were defined as those with at least 2-fold difference between two individual
718 groups at $P < 0.05$.

719

720 QUANTIFICATION AND STATISTICAL ANALYSIS

721 Statistical significance was assigned when P values were < 0.05 using Prism version 8
722 (GraphPad). Tests, number of animals (n), median values, and statistical comparison groups
723 are indicated in the Figure legends. Analysis of weight change was determined by t test or
724 one-way ANOVA with Dunnett's post-test of the area under the curve depending on the
725 number of comparison groups. Viral burden was analyzed by Mann-Whitney test when
726 comparing two groups, or one-way ANOVA or Kruskal-Wallis test with Dunnett's post-test
727 when comparing three or more groups. Cytokine data were analyzed by one-way ANOVA
728 with Tukey's multiple comparison test. qRT-PCR data were analyzed by one-way ANOVA
729 with Dunnett's post-test.

730

731

732 **REFERENCES**

733 Andreakos, E., and Tsiodras, S. (2020). COVID-19: lambda interferon against viral load and
734 hyperinflammation. *EMBO Mol Med* *12*, e12465.

735

736 Ank, N., Iversen, M.B., Bartholdy, C., Staeheli, P., Hartmann, R., Jensen, U.B.,
737 Dagnaes-Hansen, F., Thomsen, A.R., Chen, Z., Haugen, H., *et al.* (2008). An important role
738 for type III interferon (IFN-lambda/IL-28) in TLR-induced antiviral activity. *J Immunol* *180*,
739 2474-2485.

740

741 Bastard, P., Rosen, L.B., Zhang, Q., Michailidis, E., Hoffmann, H.H., Zhang, Y., Dorgham, K.,
742 Philippot, Q., Rosain, J., Beziat, V., *et al.* (2020). Autoantibodies against type I IFNs in
743 patients with life-threatening COVID-19. *Science* *370*.

744

745 Baum, A., Fulton, B.O., Wloga, E., Copin, R., Pascal, K.E., Russo, V., Giordano, S., Lanza,
746 K., Negron, N., Ni, M., *et al.* (2020). Antibody cocktail to SARS-CoV-2 spike protein
747 prevents rapid mutational escape seen with individual antibodies. *Science* *369*, 1014-1018.

748

749 Blanco-Melo, D., Nilsson-Payant, B.E., Liu, W.C., Uhl, S., Hoagland, D., Moller, R., Jordan,
750 T.X., Oishi, K., Panis, M., Sachs, D., *et al.* (2020). Imbalanced Host Response to
751 SARS-CoV-2 Drives Development of COVID-19. *Cell* *181*, 1036-1045 e1039.

752

753 Boudewijns, R., Thibaut, H.J., Kaptein, S.J.F., Li, R., Vergote, V., Seldeslachts, L., Van
754 Weyenbergh, J., De Keyzer, C., Bervoets, L., Sharma, S., *et al.* (2020). STAT2 signaling
755 restricts viral dissemination but drives severe pneumonia in SARS-CoV-2 infected hamsters.
756 *Nat Commun* *11*, 5838.

757

758 Broggi, A., Ghosh, S., Sposito, B., Spreafico, R., Balzarini, F., Lo Cascio, A., Clementi, N.,
759 De Santis, M., Mancini, N., Granucci, F., *et al.* (2020a). Type III interferons disrupt the lung
760 epithelial barrier upon viral recognition. *Science* *369*, 706-712.

761

762 Broggi, A., Granucci, F., and Zanoni, I. (2020b). Type III interferons: Balancing tissue
763 tolerance and resistance to pathogen invasion. *J Exp Med* *217*.

764

765 Broggi, A., Tan, Y., Granucci, F., and Zanoni, I. (2017). IFN-lambda suppresses intestinal
766 inflammation by non-translational regulation of neutrophil function. *Nat Immunol* *18*,
767 1084-1093.

768

769 Case, J.B., Bailey, A.L., Kim, A.S., Chen, R.E., and Diamond, M.S. (2020). Growth,
770 detection, quantification, and inactivation of SARS-CoV-2. *Virology* *548*, 39-48.

771

772 Chen, R.E., Winkler, E.S., Case, J.B., Aziati, I.D., Bricker, T.L., Joshi, A., Darling, T.L., Ying,
773 B., Errico, J.M., Shrihari, S., *et al.* (2021a). In vivo monoclonal antibody efficacy against
774 SARS-CoV-2 variant strains. *Nature* *596*, 103-108.

775
776 Chen, R.E., Zhang, X., Case, J.B., Winkler, E.S., Liu, Y., VanBlargan, L.A., Liu, J., Errico,
777 J.M., Xie, X., Suryadevara, N., *et al.* (2021b). Resistance of SARS-CoV-2 variants to
778 neutralization by monoclonal and serum-derived polyclonal antibodies. *Nat Med* 27,
779 717-726.

780
781 Diamond, M., Halfmann, P., Maemura, T., Iwatsuki-Horimoto, K., Iida, S., Kiso, M.,
782 Scheaffer, S., Darling, T., Joshi, A., Loeber, S., *et al.* (2021). The SARS-CoV-2 B.1.1.529
783 Omicron virus causes attenuated infection and disease in mice and hamsters. *Res Sq*.

784
785 Dinnon, K.H., 3rd, Leist, S.R., Schafer, A., Edwards, C.E., Martinez, D.R., Montgomery,
786 S.A., West, A., Yount, B.L., Jr., Hou, Y.J., Adams, L.E., *et al.* (2020). A mouse-adapted model
787 of SARS-CoV-2 to test COVID-19 countermeasures. *Nature* 586, 560-566.

788
789 Dobin, A., Davis, C.A., Schlesinger, F., Drenkow, J., Zaleski, C., Jha, S., Batut, P., Chaisson,
790 M., and Gingeras, T.R. (2013). STAR: ultrafast universal RNA-seq aligner. *Bioinformatics* 29,
791 15-21.

792
793 Espinosa, V., Dutta, O., McElrath, C., Du, P., Chang, Y.J., Cicciarelli, B., Pitler, A.,
794 Whitehead, I., Obar, J.J., Durbin, J.E., *et al.* (2017). Type III interferon is a critical regulator
795 of innate antifungal immunity. *Sci Immunol* 2.

796
797 Felgenhauer, U., Schoen, A., Gad, H.H., Hartmann, R., Schaubmar, A.R., Failing, K., Drosten,
798 C., and Weber, F. (2020). Inhibition of SARS-CoV-2 by type I and type III interferons. *J Biol
799 Chem* 295, 13958-13964.

800
801 Galani, I.E., Rovina, N., Lampropoulou, V., Triantafyllia, V., Manioudaki, M., Pavlos, E.,
802 Koukaki, E., Frakou, P.C., Panou, V., Rapti, V., *et al.* (2021). Untuned antiviral immunity in
803 COVID-19 revealed by temporal type I/III interferon patterns and flu comparison. *Nat
804 Immunol* 22, 32-40.

805
806 Galani, I.E., Triantafyllia, V., Eleminiadou, E.E., Koltsida, O., Stavropoulos, A., Manioudaki,
807 M., Thanos, D., Doyle, S.E., Kotenko, S.V., Thanopoulou, K., *et al.* (2017). Interferon-lambda Mediates Non-redundant Front-Line Antiviral Protection against Influenza
808 Virus Infection without Compromising Host Fitness. *Immunity* 46, 875-890 e876.

809
810 Golden, J.W., Cline, C.R., Zeng, X., Garrison, A.R., Carey, B.D., Mucker, E.M., White, L.E.,
811 Shamblin, J.D., Brocato, R.L., Liu, J., *et al.* (2020). Human angiotensin-converting enzyme 2
812 transgenic mice infected with SARS-CoV-2 develop severe and fatal respiratory disease. *JCI
813 Insight* 5.

814
815 Guan, W.J., Ni, Z.Y., Hu, Y., Liang, W.H., Ou, C.Q., He, J.X., Liu, L., Shan, H., Lei, C.L.,
816 Hui, D.S.C., *et al.* (2020). Clinical Characteristics of Coronavirus Disease 2019 in China. *N
817 Engl J Med* 382, 1708-1720.

819
820 Hoagland, D.A., Moller, R., Uhl, S.A., Oishi, K., Frere, J., Golyanek, I., Horiuchi, S., Panis,
821 M., Blanco-Melo, D., Sachs, D., *et al.* (2021). Leveraging the antiviral type I interferon
822 system as a first line of defense against SARS-CoV-2 pathogenicity. *Immunity* 54, 557-570
823 e555.

824
825 Hoffmann, M., Arora, P., Gross, R., Seidel, A., Hornich, B.F., Hahn, A.S., Kruger, N.,
826 Graichen, L., Hofmann-Winkler, H., Kempf, A., *et al.* (2021). SARS-CoV-2 variants B.1.351
827 and P.1 escape from neutralizing antibodies. *Cell* 184, 2384-2393 e2312.

828
829 Huang, C., Wang, Y., Li, X., Ren, L., Zhao, J., Hu, Y., Zhang, L., Fan, G., Xu, J., Gu, X., *et al.*
830 (2020). Clinical features of patients infected with 2019 novel coronavirus in Wuhan, China.
831 *Lancet* 395, 497-506.

832
833 Jilg, N., Lin, W., Hong, J., Schaefer, E.A., Wolski, D., Meixong, J., Goto, K., Brisac, C.,
834 Chusri, P., Fusco, D.N., *et al.* (2014). Kinetic differences in the induction of interferon
835 stimulated genes by interferon-alpha and interleukin 28B are altered by infection with
836 hepatitis C virus. *Hepatology* 59, 1250-1261.

837
838 Lazear, H.M., Schoggins, J.W., and Diamond, M.S. (2019). Shared and Distinct Functions of
839 Type I and Type III Interferons. *Immunity* 50, 907-923.

840
841 Li, Q., Nie, J., Wu, J., Zhang, L., Ding, R., Wang, H., Zhang, Y., Li, T., Liu, S., Zhang, M., *et*
842 *al.* (2021). SARS-CoV-2 501Y.V2 variants lack higher infectivity but do have immune escape.
843 *Cell* 184, 2362-2371 e2369.

844
845 Liao, Y., Smyth, G.K., and Shi, W. (2014). featureCounts: an efficient general purpose
846 program for assigning sequence reads to genomic features. *Bioinformatics* 30, 923-930.

847
848 Liu, R., Holik, A.Z., Su, S., Jansz, N., Chen, K., Leong, H.S., Blewitt, M.E., Asselin-Labat,
849 M.L., Smyth, G.K., and Ritchie, M.E. (2015). Why weight? Modelling sample and
850 observational level variability improves power in RNA-seq analyses. *Nucleic Acids Res* 43,
851 e97.

852
853 Liu, Z., VanBlargan, L.A., Bloyet, L.M., Rothlauf, P.W., Chen, R.E., Stumpf, S., Zhao, H.,
854 Errico, J.M., Theel, E.S., Liebeskind, M.J., *et al.* (2021). Identification of SARS-CoV-2 spike
855 mutations that attenuate monoclonal and serum antibody neutralization. *Cell Host Microbe* 29,
856 477-488 e474.

857
858 Major, J., Crotta, S., Llorian, M., McCabe, T.M., Gad, H.H., Priestnall, S.L., Hartmann, R.,
859 and Wack, A. (2020). Type I and III interferons disrupt lung epithelial repair during recovery
860 from viral infection. *Science* 369, 712-717.

861
862 Mehta, P., McAuley, D.F., Brown, M., Sanchez, E., Tattersall, R.S., Manson, J.J., and Hlh

863 Across Speciality Collaboration, U.K. (2020). COVID-19: consider cytokine storm
864 syndromes and immunosuppression. *Lancet* 395, 1033-1034.

865

866 Netea, M.G., Dominguez-Andres, J., Barreiro, L.B., Chavakis, T., Divangahi, M., Fuchs, E.,
867 Joosten, L.A.B., van der Meer, J.W.M., Mhlanga, M.M., Mulder, W.J.M., *et al.* (2020).
868 Defining trained immunity and its role in health and disease. *Nat Rev Immunol* 20, 375-388.

869

870 Oladunni, F.S., Park, J.G., Pino, P.A., Gonzalez, O., Akhter, A., Allue-Guardia, A.,
871 Olmo-Fontanez, A., Gautam, S., Garcia-Vilanova, A., Ye, C., *et al.* (2020). Lethality of
872 SARS-CoV-2 infection in K18 human angiotensin-converting enzyme 2 transgenic mice. *Nat
873 Commun* 11, 6122.

874

875 Palermo, E., Di Carlo, D., Sgarbanti, M., and Hiscott, J. (2021). Type I Interferons in
876 COVID-19 Pathogenesis. *Biology (Basel)* 10.

877

878 Park, A., and Iwasaki, A. (2020). Type I and Type III Interferons - Induction, Signaling,
879 Evasion, and Application to Combat COVID-19. *Cell Host Microbe* 27, 870-878.

880

881 Prokunina-Olsson, L., Alphonse, N., Dickenson, R.E., Durbin, J.E., Glenn, J.S., Hartmann, R.,
882 Kotenko, S.V., Lazear, H.M., O'Brien, T.R., Odendall, C., *et al.* (2020). COVID-19 and
883 emerging viral infections: The case for interferon lambda. *J Exp Med* 217.

884

885 Rathnasinghe, R., Jangra, S., Cupic, A., Martinez-Romero, C., Mulder, L.C.F., Kehrer, T.,
886 Yildiz, S., Choi, A., Mena, I., De Vrieze, J., *et al.* (2021). The N501Y mutation in
887 SARS-CoV-2 spike leads to morbidity in obese and aged mice and is neutralized by
888 convalescent and post-vaccination human sera. *medRxiv*.

889

890 Ritchie, M.E., Phipson, B., Wu, D., Hu, Y., Law, C.W., Shi, W., and Smyth, G.K. (2015).
891 limma powers differential expression analyses for RNA-sequencing and microarray studies.
892 *Nucleic Acids Res* 43, e47.

893

894 Robinson, M.D., McCarthy, D.J., and Smyth, G.K. (2010). edgeR: a Bioconductor package
895 for differential expression analysis of digital gene expression data. *Bioinformatics* 26,
896 139-140.

897

898 Schneider, W.M., Chevillotte, M.D., and Rice, C.M. (2014). Interferon-stimulated genes: a
899 complex web of host defenses. *Annu Rev Immunol* 32, 513-545.

900

901 Schreiber, G. (2020). The Role of Type I Interferons in the Pathogenesis and Treatment of
902 COVID-19. *Front Immunol* 11, 595739.

903

904 Shindo, H., Maekawa, S., Komase, K., Miura, M., Kadokura, M., Sueki, R., Komatsu, N.,
905 Shindo, K., Amemiya, F., Nakayama, Y., *et al.* (2013). IL-28B (IFN-lambda3) and IFN-alpha
906 synergistically inhibit HCV replication. *J Viral Hepat* 20, 281-289.

907

908 Shuai, H., Chan, J.F., Yuen, T.T., Yoon, C., Hu, J.C., Wen, L., Hu, B., Yang, D., Wang, Y.,
909 Hou, Y., *et al.* (2021). Emerging SARS-CoV-2 variants expand species tropism to murines.
910 EBioMedicine 73, 103643.

911

912 Sohn, S.Y., Hearing, J., Mugavero, J., Kirillov, V., Gorbunova, E., Helminiak, L., Mishra, S.,
913 Mackow, E., Hearing, P., Reich, N.C., *et al.* (2021). Interferon-Lambda Intranasal Protection
914 and Differential Sex Pathology in a Murine Model of SARS-CoV-2 Infection. mBio 12,
915 e0275621.

916

917 Sposito, B., Broggi, A., Pandolfi, L., Crotta, S., Clementi, N., Ferrarese, R., Sisti, S.,
918 Criscuolo, E., Spreafico, R., Long, J.M., *et al.* (2021). The interferon landscape along the
919 respiratory tract impacts the severity of COVID-19. Cell 184, 4953-4968 e4916.

920

921 Stanifer, M.L., Kee, C., Cortese, M., Zumaran, C.M., Triana, S., Mukenhirn, M., Kraeusslich,
922 H.G., Alexandrov, T., Bartenschlager, R., and Boulant, S. (2020). Critical Role of Type III
923 Interferon in Controlling SARS-CoV-2 Infection in Human Intestinal Epithelial Cells. Cell
924 Rep 32, 107863.

925

926 Tegally, H., Wilkinson, E., Giovanetti, M., Iranzadeh, A., Fonseca, V., Giandhari, J., Doolabh,
927 D., Pillay, S., San, E.J., Msomi, N., *et al.* (2021). Detection of a SARS-CoV-2 variant of
928 concern in South Africa. Nature 592, 438-443.

929

930 van der Wijst, M.G.P., Vazquez, S.E., Hartoularos, G.C., Bastard, P., Grant, T., Bueno, R., Lee,
931 D.S., Greenland, J.R., Sun, Y., Perez, R., *et al.* (2021). Type I interferon autoantibodies are
932 associated with systemic immune alterations in patients with COVID-19. Sci Transl Med 13,
933 eabh2624.

934

935 VanBlargan, L.A., Errico, J.M., Halfmann, P.J., Zost, S.J., Crowe, J.E., Jr., Purcell, L.A.,
936 Kawaoka, Y., Corti, D., Fremont, D.H., and Diamond, M.S. (2022). An infectious
937 SARS-CoV-2 B.1.1.529 Omicron virus escapes neutralization by therapeutic monoclonal
938 antibodies. Nature Medicine.

939

940 Vanderheiden, A., Ralfs, P., Chirkova, T., Upadhyay, A.A., Zimmerman, M.G., Bedoya, S.,
941 Aoued, H., Tharp, G.M., Pellegrini, K.L., Manfredi, C., *et al.* (2020). Type I and Type III
942 Interferons Restrict SARS-CoV-2 Infection of Human Airway Epithelial Cultures. J Virol 94,
943

944 Winkler, E.S., Bailey, A.L., Kafai, N.M., Nair, S., McCune, B.T., Yu, J., Fox, J.M., Chen,
945 R.E., Earnest, J.T., Keeler, S.P., *et al.* (2020). SARS-CoV-2 infection of human
946 ACE2-transgenic mice causes severe lung inflammation and impaired function. Nat Immunol
947 21, 1327-1335.

948

949 Winkler, E.S., Chen, R.E., Alam, F., Yildiz, S., Case, J.B., Uccellini, M.B., Holtzman, M.J.,
950 Garcia-Sastre, A., Schotsaert, M., and Diamond, M.S. (2021). SARS-CoV-2 causes lung

951 infection without severe disease in human ACE2 knock-in mice. *J Virol*, JVI0151121.

952

953 Zhang, L., Cui, Z., Li, Q., Wang, B., Yu, Y., Wu, J., Nie, J., Ding, R., Wang, H., Zhang, Y., *et*
954 *al.* (2021a). Ten emerging SARS-CoV-2 spike variants exhibit variable infectivity, animal
955 tropism, and antibody neutralization. *Commun Biol* 4, 1196.

956

957 Zhang, W., Zhao, Y., Zhang, F., Wang, Q., Li, T., Liu, Z., Wang, J., Qin, Y., Zhang, X., Yan,
958 X., *et al.* (2020). The use of anti-inflammatory drugs in the treatment of people with severe
959 coronavirus disease 2019 (COVID-19): The Perspectives of clinical immunologists from
960 China. *Clin Immunol* 214, 108393.

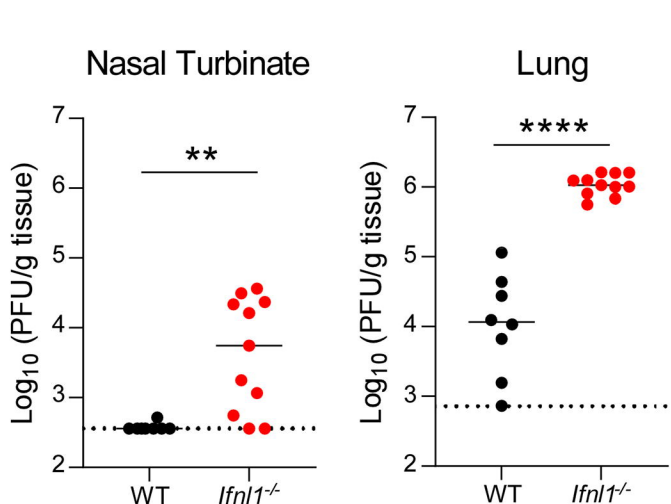
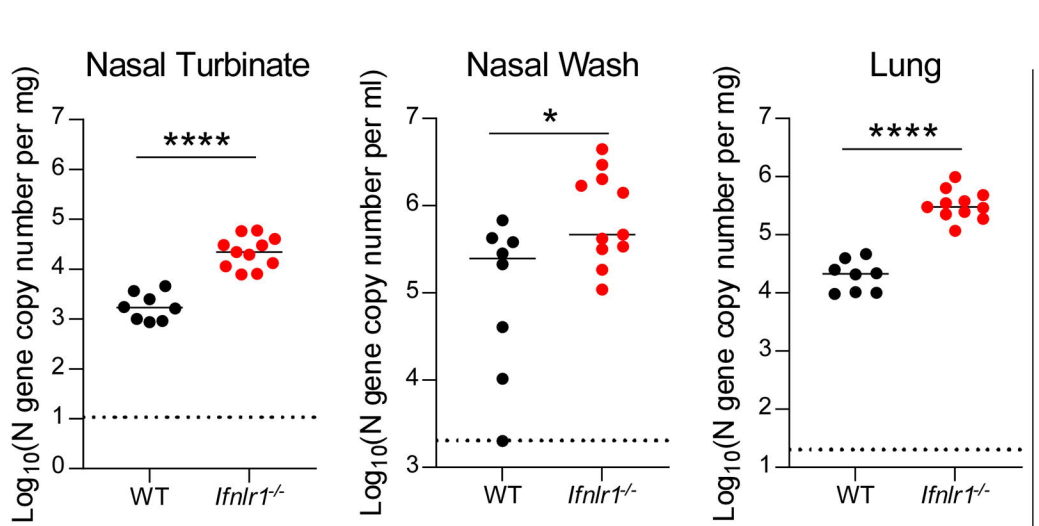
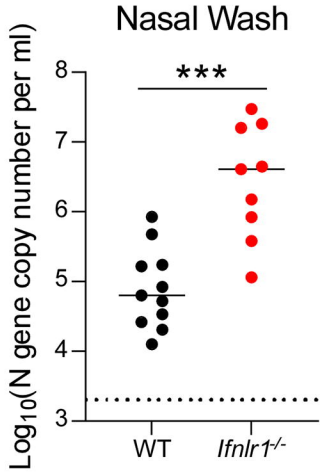
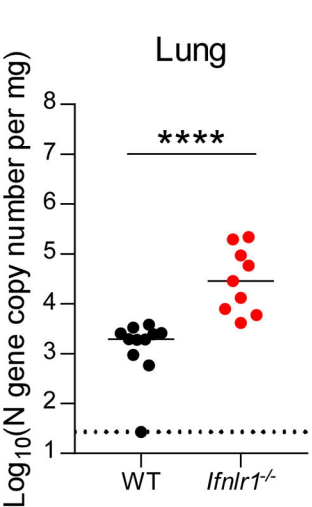
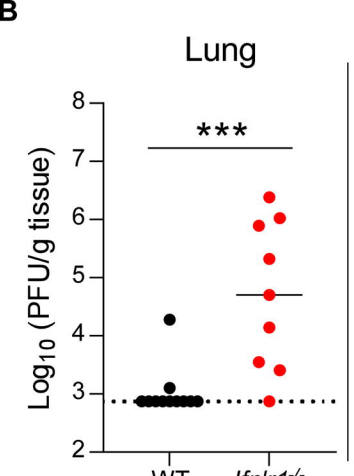
961

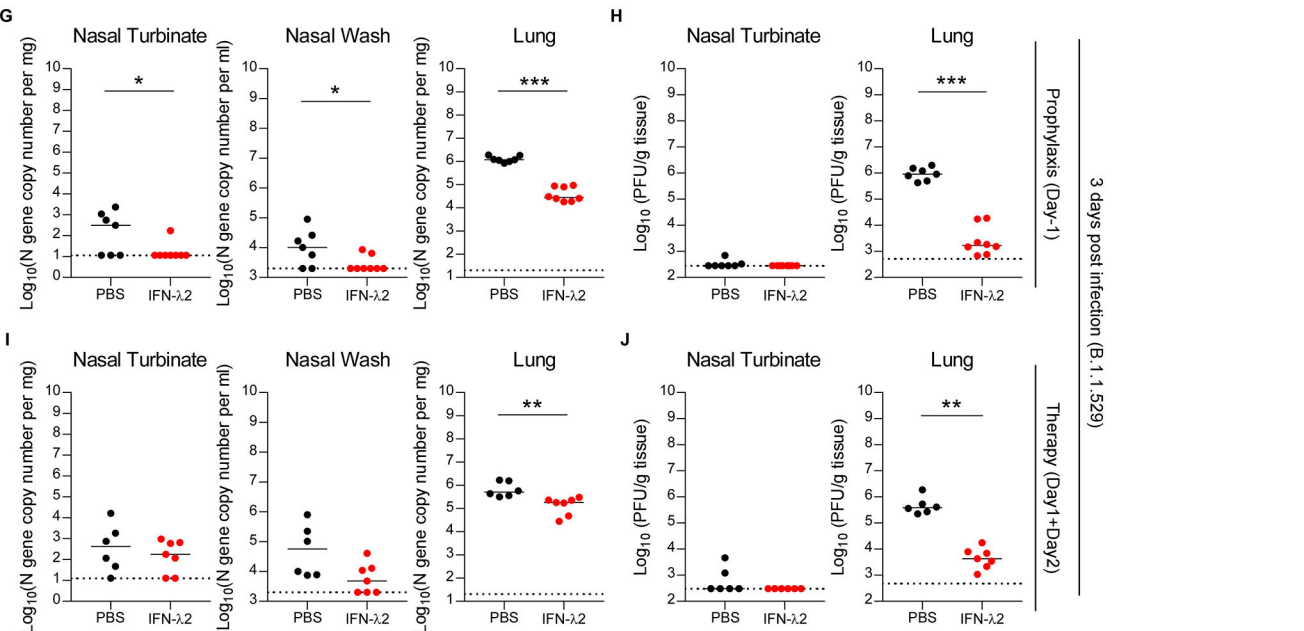
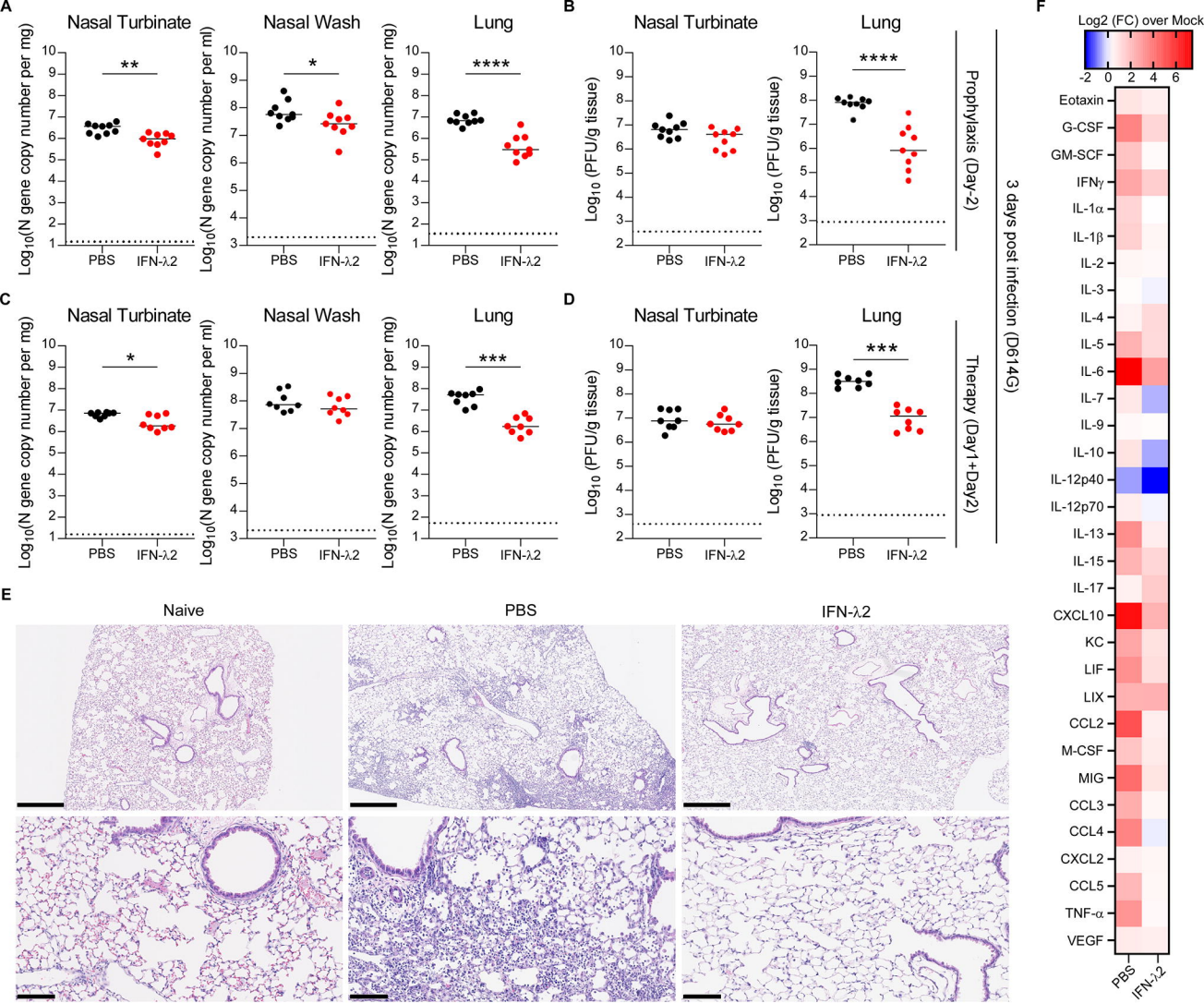
962 Zhang, X., Wu, S., Wu, B., Yang, Q., Chen, A., Li, Y., Zhang, Y., Pan, T., Zhang, H., and He,
963 X. (2021b). SARS-CoV-2 Omicron strain exhibits potent capabilities for immune evasion and
964 viral entrance. *Signal Transduct Target Ther* 6, 430.

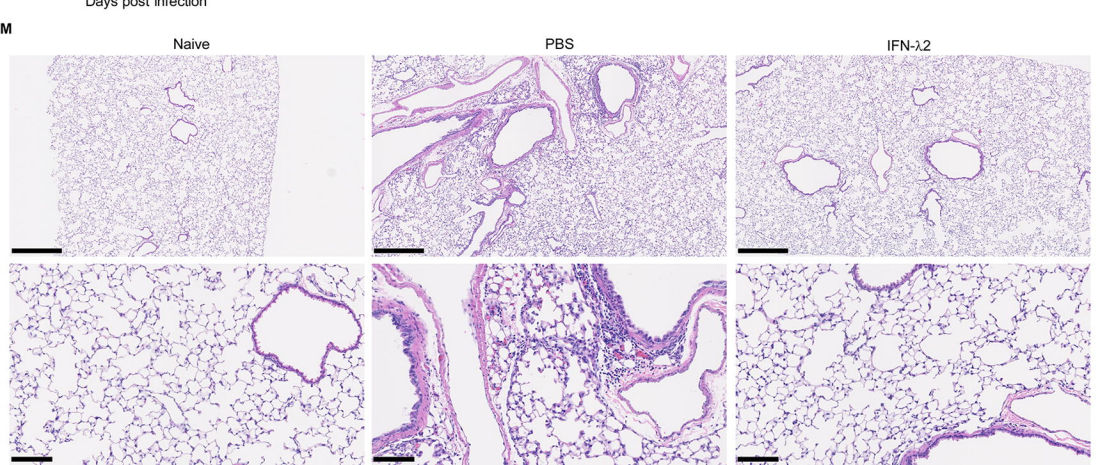
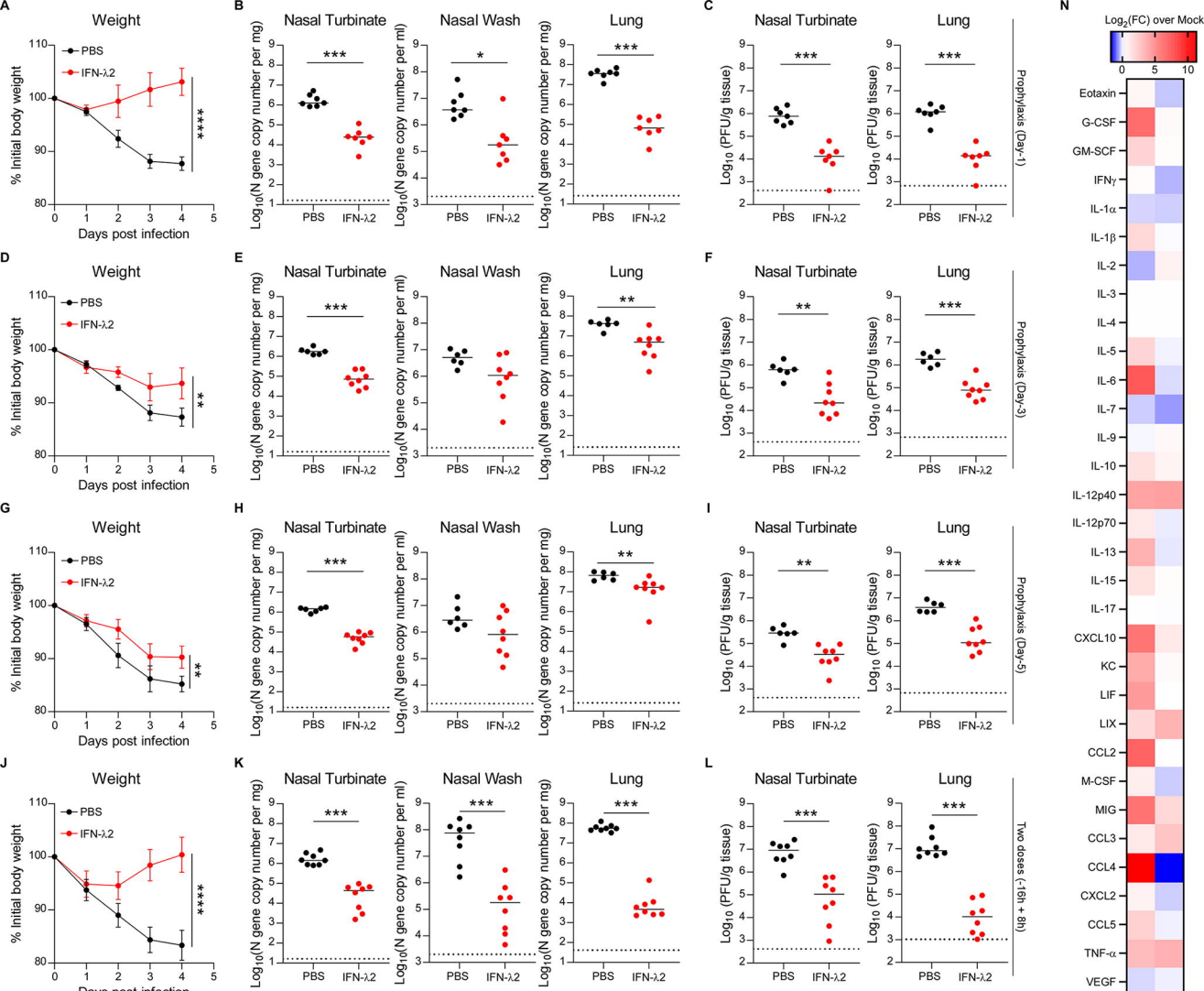
965

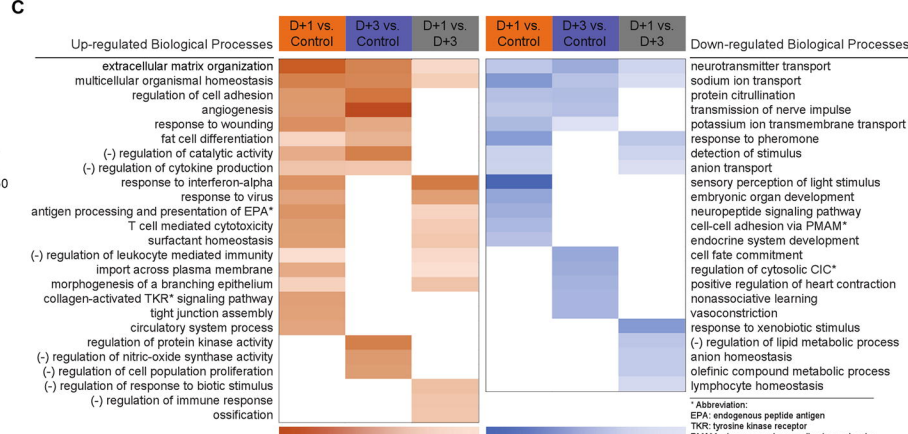
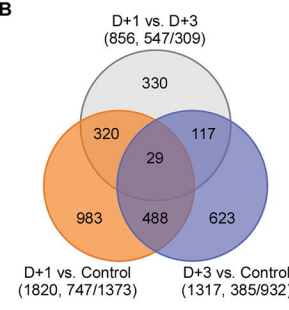
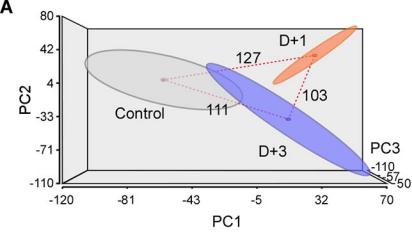
966 Ziegler, C.G.K., Allon, S.J., Nyquist, S.K., Mbano, I.M., Miao, V.N., Tzouanas, C.N., Cao, Y.,
967 Yousif, A.S., Bals, J., Hauser, B.M., *et al.* (2020). SARS-CoV-2 Receptor ACE2 Is an
968 Interferon-Stimulated Gene in Human Airway Epithelial Cells and Is Detected in Specific
969 Cell Subsets across Tissues. *Cell* 181, 1016-1035 e1019.

970









* Abbreviation:
 EPA: endogenous peptide antigen
 TKR: tyrosine kinase receptor
 PMAM: plasma-membrane adhesion molecules
 Cic: calcium ion concentration

